Supplementary Data

Single molecule study of the CUG repeat·MBNL1 interaction and its inhibition by small molecules

Amin Haghighat Jahromi[1,2], Masayoshi Honda[3,] , Steven C. Zimmerman[2,*] & Maria Spies[,3,,*]

[1]Center for Biophysics and Computational Biology, University of Illinois, Urbana, IL, USA

[2]Department of Chemistry, University of Illinois, Urbana, IL, USA

[3]Department of Biochemistry, University of Iowa Carver College of Medicine, Iowa City, IA, USA

* To whom correspondence should be addressed. Maria Spies, Tel: +1-319-335-7932 Fax: +1-319-335-9570; Email: mspies@uiowa.edu. Correspondence may also be addressed to Steven C. Zimmerman. Tel: +1-217-333-6655; Email: sczimmer@illinois.edu

Supplementary Results

Supplementary Figures

Supplementary Figure S1 (Synthesis of Ligand **1**)…… Page S3
Supplementary Figure S2 (Synthesis of linker chain in Ligand **2**)……..…Page S5
Supplementary Figure S3 (Synthesis of Ligand **2**)…….Page S7
Supplementary Figure S4 (Representative single molecule trajectories)..……...Page S13
Supplementary Figure S5 (Global fitting of off-event dwell time for **1**)……Page S14
Supplementary Figure S6 (Global fitting of on-event dwell time for **1**)……Page S15
Supplementary Figure S7 (Global fitting of off-event dwell time for **2**)……Page S16
Supplementary Figure S8 (Global fitting of on-event dwell time for **2**)……Page S17
Supplementary Figure S9 (Single molecule study with unlabeled MBNL1)..……Page S18
Supplementary Figure S10 (Stoichiometric study of MBNL1·$(CUG)_{12}$ by SPR)..……Page S20
Supplementary Figure S11 (SPR sensograms and fitting data)……..……Page S21
Supplementary Figure S12 (ITC binding study of **1** and **2** to MBNL1)……....……Page S23

Supplementary Notes

Supplementary Note 1 (Assumptions for single molecule data analysis)……...Page S10
Supplementary Note 2 (Deriving apparent IC_{50} values from single molecule data).....Page S10
Supplementary Note 3 (Details of SPR experimental design)…….....Page S19
Supplementary Note 4 (Application of ITC experiment)…..…….....Page S23
Supplementary Note 5 (Sequences and modifications of RNA constructs)….....Page S24

Supplementary Methods (SPR and ITC experimental methods) ……Page S25

Supplementary References ……..……...…..……Page S26

NMR spectra of compounds……..……...…Page S27

Supplementary Results

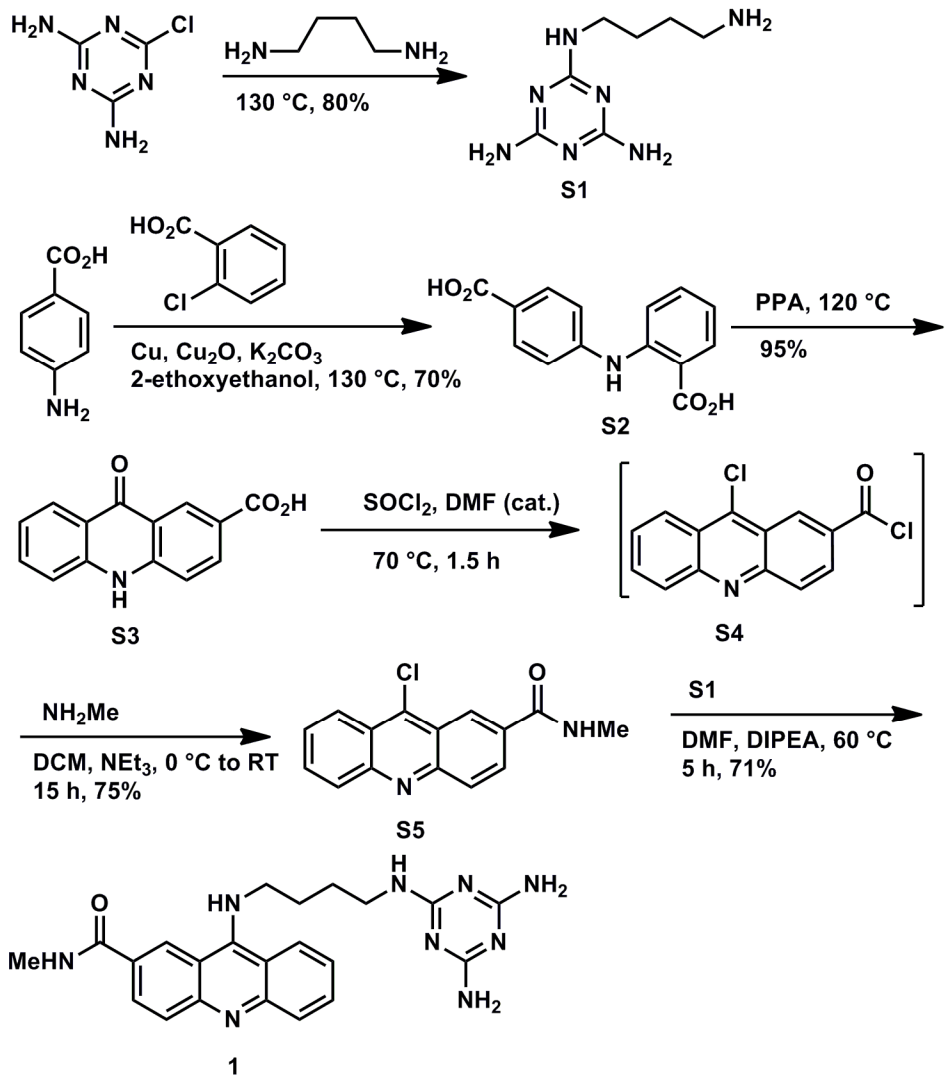

Supplementary Figure S1. Synthesis of 9-((4-((4,6-Diamino-1,3,5-triazin-2-yl)amino)butyl)amino)-*N*-methylacridine-2-carboxamide (**1**).

***N*2-(4-Aminobutyl)-1,3,5-triazine-2,4,6-triamine (S1).** Title compound was prepared as described previously (1), in 80% yield. ^{1}H NMR (500 MHz, DMSO-d_6) δ 6.40 (t, J = 5.6 Hz, 1H), 6.05 (s, 2H), 5.88 (s, 2H), 3.14 (q, J = 6.3 Hz, 2H), 2.54 – 2.52 (m, 2H), 1.44 (p, J = 7.1 Hz, 2H), 1.37 – 1.31 (m, 2H).

2-((4-Carboxyphenyl)amino)benzoic acid (S2). Title compound was prepared as described previously (2), with minor changes in the work-up procedure, in 70% yield. ^{1}H NMR (500 MHz, DMSO-*d*$_6$) δ 9.87 (bs, 1H), 7.94 (d, J = 8.0 Hz, 1H), 7.87 (d, J = 8.7 Hz, 2H), 7.50 – 7.46 (m, 2H), 7.27 (d, J = 8.7 Hz, 2H), 6.96 – 6.91 (m, 1H).; m/z LRMS (ESI) calculated for [M+H]+: 258.1; found 258.1.

9-Oxo-9,10-dihydroacridine-2-carboxylic acid (S3). Title compound was prepared as described previously (3), with minor changes in the work-up procedure, in 95% yield. ^{1}H NMR (400 MHz, DMSO-*d*$_6$) δ 12.90 (bs, 1H), 12.06 (s, 1H), 8.83 (d, J = 2.0 Hz, 1H), 8.22 (ddd, J = 17.7, 8.4, 1.6 Hz, 2H), 7.8 – 7.76 (m, 1H), 7.6 – 7.57 (m, 2H), 7.36 – 7.27 (m, 1H); ^{13}C NMR (125 MHz, DMSO-*d*$_6$) δ 177.00, 167.41, 143.13, 140.90, 134.12, 133.88, 133.62, 128.38, 126.10, 121.76, 120.85, 119.69, 117.69, 117.38; m/z LRMS (ESI) calculated for [M+H]+: 240.1; found 240.1.

9-Chloro-*N*-methylacridine-2-carboxamide (S5). A round-bottom flask, equipped with a stir bar, was charged with **S3** (375 mg, 1.6 mmol, 1 eq) and freshly distilled thionyl chloride (2 mL, 27.5 mmol , 17.2 eq). A catalytic amount of DMF was added and the solution was heated gently under reflux at 69 ºC, stirring until homogeneous and then for 1 h. The excess thionyl chloride was distilled off and the last traces were removed azeotropically via coevaporation with DCM (3 x 50 mL). The mixture was left under vacuum (minimally) for 1 hr to afford the crude intermediate, **S4**, as a yellow powder. ^{1}H NMR (500 MHz, chloroform-*d*) δ 9.48 (d, J = 1.5 Hz, 1H), 9.25 (d, J = 9.2 Hz, 1H), 9.16 (d, J = 8.8 Hz, 1H), 8.72 – 8.62 (m, 2H), 8.37 – 8.30 (m, 1H), 8.06 – 7.99 (m, 1H); *m/z* LRMS (ESI) calculated for $[M+H]^+$: 276.0; found 276.0. The crude intermediate, without further purification, was dissolved in anhydrous DCM. Anhydrous triethylamine was added to the solution until the pH = 11 and it was cooled to 0 ºC. A 2M solution of methylamine in methanol (0.9 mL, 1.8 mmol, 1.1 eq) was added and the solution was stirred at 0 ºC for 2 h and then slowly warmed to room temperature overnight. The solvent was removed by rotary evaporation and the crude mixture was purified via flash chromatography (SiO_2; CH_2Cl_2:MeOH, 98:2 to 95:5) to yield a yellow solid (325 mg, 1.2 mmol, 75%). ^{1}H NMR (500 MHz, chloroform-*d*) δ 8.79 (d, J = 1.6 Hz, 1H), 8.40 (d, J = 8.6 Hz, 1H), 8.24 – 8.19 (m, 2H), 8.14 (dd, J = 9.0, 1.8 Hz, 1H), 7.86 – 7.83 (m, 1H), 7.69 – 7.62 (m, 1H), 6.56 (bs, 1H), 3.13 (d, J = 4.8 Hz, 3H); *m/z* LRMS (ESI) calculated for $[M+H]^+$: 271.1; found 271.1.

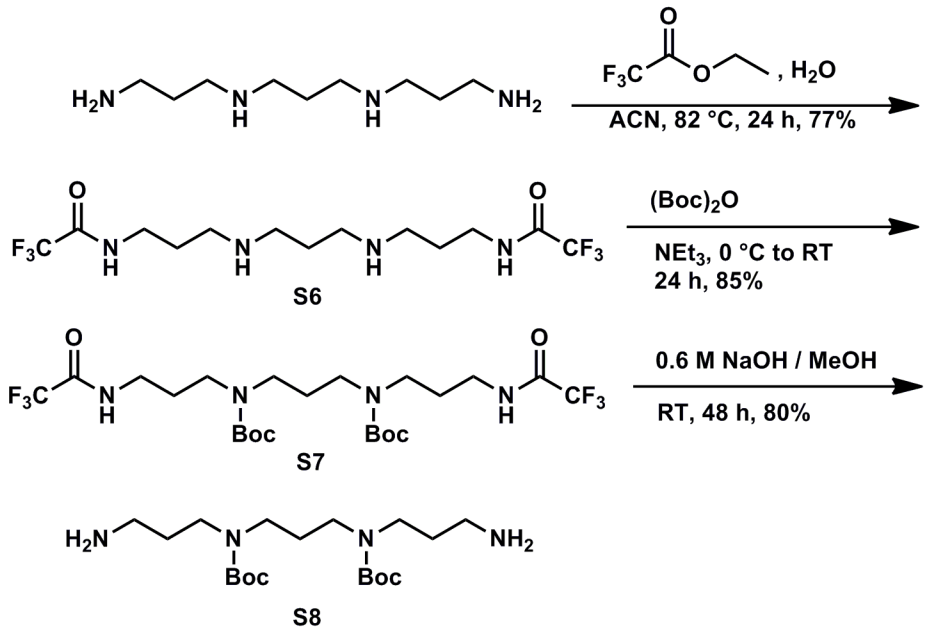

Supplementary Figure S2 . Synthesis of Di-tert-Butyl propane-1,3-diylbis((3-aminopropyl)carbamate (S8).

***N,N'*-((Propane-1,3-diylbis(azanediyl))bis(propane-3,1-diyl))bis(2,2,2-trifluoroacetamide) (S6).** The title compound was prepared from *N*1,*N*1'-(propane-1,3-diyl)bis(propane-1,3-diamine) as described previously[4], with minor changes, in 77% yield. ^{1}H NMR (500 MHz, DMSO-d_6) δ 9.61 (s, 2H), 8.75 (bs, 2H), 3.26 (q, J = 6.5 Hz, 4H), 3.02 – 2.95 (m, 4H), 2.94 – 2.88 (m, 4H), 1.91 (p, J = 7.8 Hz, 2H), 1.82 (p, J = 7.0 Hz, 4H); ^{13}C NMR (125 MHz, DMSO-d_6) δ 156.40, 117.08, 44.63, 44.02, 36.61, 25.22, 22.56; *m/z* LRMS (ESI) calculated for $[M+H]^+$: 381.2; found 381.2.

Di-*tert*-Butyl propane-1,3-diylbis((3-(2,2,2-trifluoroacetamido)propyl)carbamate) (S7). The title compound was prepared as described previously[4], with minor changes. The product was purified via flash chromatography (SiO_2; CH_2Cl_2:MeOH, 98:2 to 95:5) to afford S7 in 85% yield. ^{1}H NMR (500 MHz, DMSO-d_6) δ 9.42 (bs, 2H), 3.18 – 3.07 (m, 12H), 1.71 – 1.60 (m, 6H), 1.37 (s, 18H); *m/z* LRMS (ESI) calculated for $[M+H]^+$: 581.3; found 581.3.

Di-*tert*-Butyl propane-1,3-diylbis((3-aminopropyl)carbamate (S8). The title compound was prepared as described previously (4), with minor changes. The product was purified via flash chromatography (SiO_2; CH_2Cl_2:MeOH:NH_4OH, 80:19:1 to 67:30:2) to afford S8 in 80% yield.

^{1}H NMR (500 MHz, chloroform-*d*) δ 3.28 (s, 4H), 3.16 (s, 4H), 2.69 (t, J = 6.4 Hz, 4H), 1.75 (s, 2H), 1.64 (p, J = 6.8 Hz, 4H), 1.45 (s, 18H); ^{13}C NMR (126 MHz, chloroform-*d*) δ 155.29, 79.06, 44.44, 43.68, 38.96, 32.34, 31.73, 28.17; *m/z* LRMS (ESI) calculated for $[M+H]^{+}$: 389.3; found 389.3.

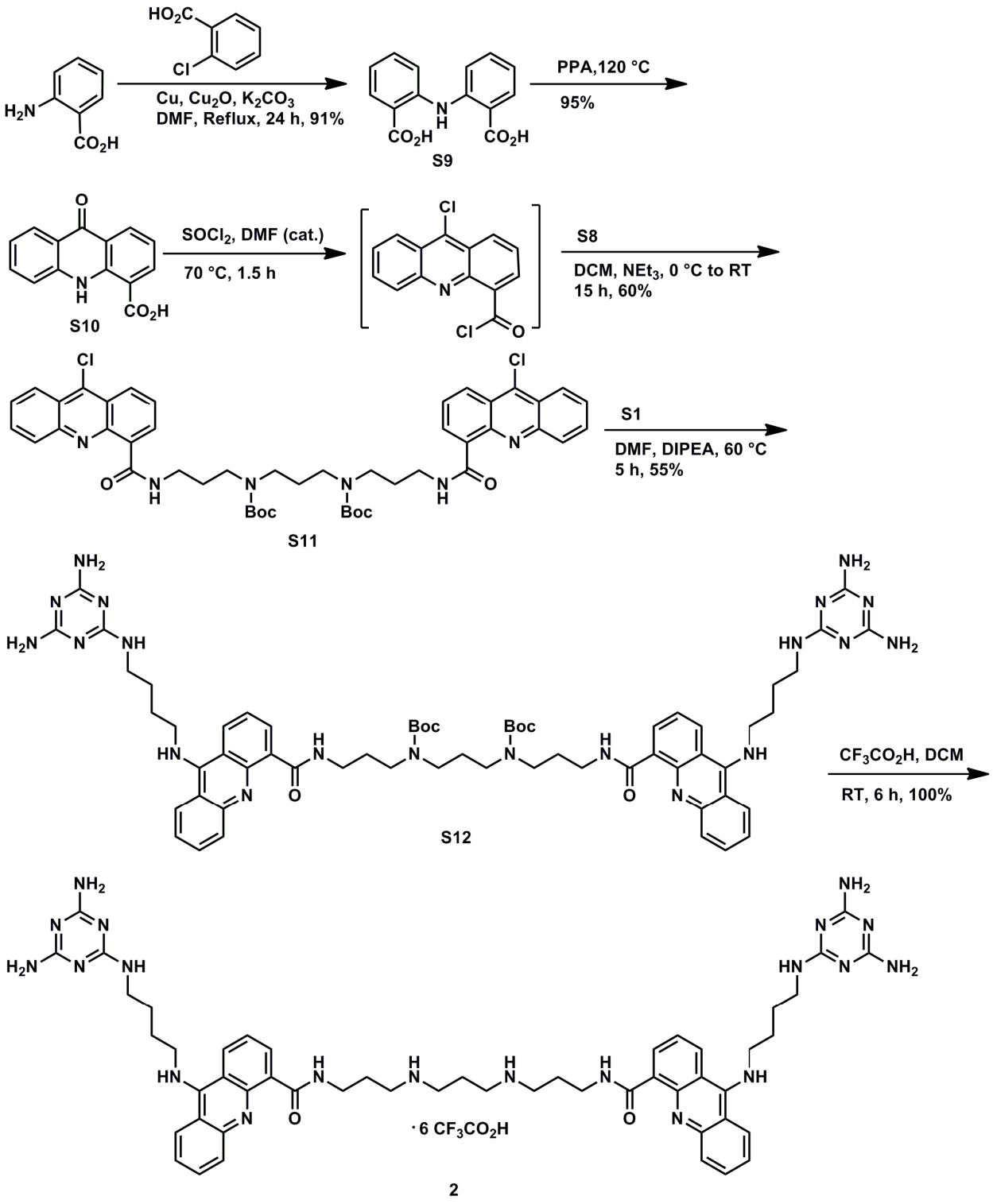

Supplementary Figure S3. Synthesis of *N,N′*-((Propane-1,3-diylbis(azanediyl))bis(propane-3,1-diyl))bis(9-((4-((4,6-diamino-1,3,5-triazin-2-yl)amino)butyl)amino)acridine-4-carboxamide) (2).

2,2'-Iminodibenzoic (S9). A round-bottom flask, equipped with a stir bar, was charged with 2-bromobenzoic acid (3.00 g, 14.9 mmol, 1 eq), anthranilic acid (2.25 g, 16.4 mmol, 1.1 eq), K_2CO_3 (6.00 g, 44 mmol, 2.95 eq), Cu (0.20 g, 2.9 mmol, 0.2 eq) and Cu_2O (0.22 g, 1.45 mmol, 0.1 eq). To this mixture, anhydrous DMF (50 mL) was added and it was stirred at reflux at 130 ºC for 16 h. The work-up procedure was carried out as reported previously (5), to yield 2,2'-iminodibenzoic acid in 91% yield as a light green solid. ^{1}H NMR (400 MHz, DMSO-*d*$_6$) δ 13.06 (bs, 1H), 10.85 (bs, 1H), 7.91 (s, 2H), 7.46 (s, 4H), 6.95 (s, 2H); ^{13}C NMR (100 MHz, DMSO-*d*$_6$) δ 168.41, 143.58, 133.38, 131.81, 119.99, 117.56, 113.56; *m/z* LRMS (ESI) calculated for $[M+H]^+$: 258.1; found 258.1.

9-Oxo-9,10-dihydroacridine-4-carboxylic acid (S10). The title compound was prepared as described previously[3], with minor changes in the work-up procedure, in 95% yield. ^{1}H NMR (500 MHz, DMSO-*d*$_6$) δ 11.96 (s, 1H), 8.53 (dd, J = 8.0, 1.5 Hz, 1H), 8.45 (dd, J = 7.5, 1.7 Hz, 1H), 8.24 (d, J = 8.1 Hz, 1H), 7.82 – 7.73 (m, 2H), 7.39 – 7.30 (m, 2H); ^{13}C NMR (125 MHz, DMSO-*d*$_6$) δ 176.53, 169.14, 141.20, 139.92, 136.90, 134.11, 132.41, 125.89, 122.32, 121.63, 120.60, 120.24, 118.63, 115.01; *m/z* LRMS (ESI) calculated for $[M+H]^+$: 240.1; found 240.1.

Di-*tert*-Butylpropane-1,3-diylbis((3-(9-chloroacridine-4-carboxamido)propyl)carbamate) (S11). A round-bottom flask equipped with a stir bar was charged with **S10** (600 mg, 2.5 mmol, 1 eq) and freshly distilled thionyl chloride (3 mL, 41 mmol , 16.4 eq). A catalytic amount of DMF was added and heated gently under reflux at 69 ºC, stirring until homogeneous and then for 1 h. The excess thionyl chloride was distilled off and the last traces removed azeotropically via coevaporation with DCM (3 x 50 mL). It was left under vacuum for (minimally) 1 h to afford the crude intermediate as a yellow powder. The crude intermediate was dissolved in anhydrous DCM. Anhydrous triethylamine was added to the solution until the pH was 11 and it was cooled to 0 ºC. **S8** (437 mg, 1.125 mmol, 0.45 eq) was added and the solution was stirred at 0 ºC for 2 h and slowly warmed to room temperature overnight. The solvent was removed by rotary evaporation and the crude mixture was purified via flash chromatography (SiO_2; CH_2Cl_2:MeOH, 98:2 to 95:5) to yield a yellow solid (586 mg, 0.675 mmol, 60%). ^{1}H NMR (500 MHz, chloroform-*d*) δ 9.00 (s, 2H), 8.36 (d, J = 14.0 Hz, 4H), 8.27 (s, 2H), 8.20 (d, J = 16.2 Hz, 4H), 7.80 (s, 2H), 7.65 – 7.60 (m, 2H), 3.54 (s, 4H), 3.46 (d, J = 12.0 Hz, 4H), 3.23 (s, 4H), 1.86 (dd, J = 14.5, 7.5 Hz, 6H), 1.52 (s, 18H); ^{13}C NMR (125 MHz, chloroform-*d*) δ 166.30, 156.65, 149.56,

149.23, 142.50, 132.76, 131.12, 130.12, 129.75, 128.54, 127.13, 124.59, 124.33, 123.26, 80.31, 44.94, 43.54, 36.14, 28.52, 27.87, 27.63; *m/z* LRMS (ESI) calculated for $[M+H]^+$: 867.3; found 867.3.

Di-*tert*-Butylpropane-1,3-diylbis((3-(9-((4-((4,6-diamino-1,3,5-triazin-2-yl)amino)butyl)amino)acridine-4-carboxamido)propyl)carbamate) (S12). A round-bottom flask, equipped with a stir bar, was charged with **S11** (500 mg, 0.576 mmol, 1 eq) and *N*2-(4-aminobutyl)-1,3,5-triazine-2,4,6-triamine (250 mg, 1.27 mmol, 2.2 eq). DIPEA (327 mg, 2.53 mmol, 4.4 eq) and anhydrous DMF (25 mL) were added. The solution was heated at 70 ºC for 5 h. The solvent was removed by rotary evaporation and the product purified via flash chromatography (basic alumina; DCM:methanol:NH_4OH, from 95:4.9:0.1 to 90:9.5:0.5) to yield a yellow solid (377 mg, 0.317 mmol, 55%).^{1}H NMR (500 MHz, methanol-d_4) δ 8.60 (s, 2H), 8.37 (d, J = 8.5 Hz, 2H), 8.20 (d, J = 8.5 Hz, 2H), 7.96 – 7.76 (m, 2H), 7.63 (s, 2H), 7.37 – 7.27 (m, 4H), 3.82 (s, 4H), 3.49 (s, 4H), 3.35 (s, 4H), 3.27 (t, J = 6.8 Hz, 4H), 3.19 (s, 4H), 1.94 – 1.76 (m, 10H), 1.59 (d, J = 7.0 Hz, 4H), 1.34 (d, J = 35.9 Hz, 18H); *m/z* LRMS (ESI) calculated for $[M+H]^+$: 1189.7; found 1189.7.

Supplementary Note 1

$K_{D2} = \frac{k_{-2}}{k_{+2}} = \frac{\left[RNA^{free}\right] \times [I]}{[RNA \bullet I]}$, is the equilibrium dissociation constant for ligand (**1** or **2**) binding to $(CUG)_4$. Free and ligand-bound RNA exist in equilibrium defined by K_{D2} and ligand concentration. All single-molecule TIRFM studies were carried out under conditions where the concentration of the inhibitor was much greater than was the concentration of surface-tethered RNA. Hence, it can be safely assumed that the total concentration of ligand equals the concentration of free ligand and is designated as [I] below. The second assumption is that only a small fraction of the protein is in the RNA·P or RNA·I·P complex because its concentration in the microscope flow cell is significantly lower than the expected K_{D1} or K_{D3}. The binding kinetics can be then deduced from the ON time distributions analyzed using the open scheme shown in Table. 1b where the forward flux through the two manifolds will be determine by this ratio:

$$\frac{[RNA^{free}]}{[RNA \bullet I]} = \frac{K_D^I}{[I]} = \frac{flux(1)}{flux(2)}$$

Supplementary Note 2

Because of the kinetic scheme, which includes two pathways, we cannot use the traditional definition of K_I. We can, however, define the apparent IC_{50} as a concentration of the ligand at which 50% of MBNL1 is free.

Apparent $IC_{50} = I^{50}$; MBNL1 protein and $(CUG)_4$ are shown as P and RNA, respectively.

Total protein concentration $\left[P^{total}\right] = \left[P^{FREE}\right] + [RNA \cdot P] + [RNA \cdot I \cdot P] = P;$

Total RNA $\left[RNA^{total}\right] = \left[RNA^{FREE}\right] + [RNA \cdot I] + [RNA \cdot P] + [RNA \cdot I \cdot P] = R.$

We need to express IC_{50} in terms of known concentrations and equilibrium dissociation constants:

$$\begin{cases} (1)[P^{FREE}] = [RNA \cdot P] + [RNA \cdot I \cdot P] = \dfrac{P}{2} \\ (2) K_{D1} \times [RNA \cdot P] = [RNA^{FREE}] \times \dfrac{P}{2} \\ (3) K_{D3} \times [RNA \cdot I \cdot P] = [RNA \cdot I] \times \dfrac{P}{2} \\ (4) K_{D2} \times [RNA \cdot I] = [RNA^{FREE}] \times I^{50} \\ (5) R = [RNA^{FREE}] + [RNA \cdot I] + [RNA \cdot P] + [RNA \cdot I \cdot P] = [RNA^{FREE}] + [RNA \cdot I] + \dfrac{P}{2} \end{cases}$$

$$(4) \rightarrow [RNA \cdot I] = \frac{[RNA^{FREE}] \times I^{50}}{K_{D2}}$$

$$(5)\,\&\,(4) \rightarrow [RNA^{FREE}] + [RNA^{FREE}] \times \frac{I^{50}}{K_{D2}} = R - \frac{P}{2}$$

$$[RNA^{FREE}] = \frac{K_{D2} \times \left(R - \dfrac{P}{2} \right)}{K_{D2} + I^{50}} \quad (6)$$

$$(3)\,\&\,(4) \rightarrow [RNA \cdot I] = \frac{K_{D3} \times [RNA \cdot I \cdot P]}{\dfrac{P}{2}} = \frac{[RNA^{FREE}] \times I^{50}}{K_{D2}}$$

$$(1) \rightarrow [RNA \cdot I \cdot P] = \frac{P}{2} - [RNA \cdot P] \underset{\frac{P}{2}}{=} \frac{P}{2} - \frac{[RNA^{FREE}] \times \dfrac{P}{2}}{K_{D1}} = \frac{P}{2} \times \frac{K_{D1} - [RNA^{FREE}]}{K_{D1}}$$

$$[RNA \cdot I \cdot P] = \frac{\dfrac{P}{2} \times [RNA^{FREE}] \times I^{50}}{K_{D3} \times K_{D2}} = \frac{P}{2} \times \frac{K_{D1} - [RNA^{FREE}]}{K_{D1}}$$

$$K_{D1} \times K_{D2} \times K_{D3} - K_{D2} \times K_{D3} \times [RNA^{FREE}] = K_{D1} \times [RNA^{FREE}] \times I^{50}$$

$$[RNA^{FREE}] \times \left(K_{D1} \times I^{50} + K_{D2} \times K_{D3} \right) = K_{D1} \times K_{D2} \times K_{D3}$$

$$[RNA^{FREE}] = \frac{K_{D1} \times K_{D2} \times K_{D3}}{\left(K_{D1} \times I^{50} + K_{D2} \times K_{D3} \right)} \quad (7)$$

$$(6)\,\&\,(7) \rightarrow \frac{K_{D1} \times K_{D2} \times K_{D3}}{K_{D1} \times I^{50} + K_{D2} \times K_{D3}} = \frac{K_{D2} \times \left(R - \frac{P}{2} \right)}{K_{D2} + I^{50}}$$

$$\left(K_{D2} + I^{50} \right) \times K_{D1} \times K_{D3} = \left(K_{D1} \times I^{50} + K_{D2} \times K_{D3} \right) \times \left(R - \frac{P}{2} \right)$$

$$I^{50} \times K_{D1} \times K_{D3} + K_{D1} \times K_{D2} \times K_{D3} = I^{50} \times K_{D1} \times \left(R - \frac{P}{2} \right) + K_{D3} \times K_{D2} \times \left(R - \frac{P}{2} \right)$$

$$I^{50} \times \left(K_{D1} \times K_{D3} - K_{D1} \times \left(R - \frac{P}{2} \right) \right) = K_{D3} \times K_{D2} \times \left(R - \frac{P}{2} \right) - K_{D1} \times K_{D2} \times K_{D3}$$

$$I^{50} = \frac{K_{D2} \times K_{D3} \times \left(R - \frac{P}{2} \right) - K_{D1} \times K_{D2} \times K_{D3}}{\left(K_{D1} \times K_{D3} - K_{D1} \times \left(R - \frac{P}{2} \right) \right)} \qquad (8)$$

Equation (8) relates the apparent IC_{50} to the absolute concentrations of protein and RNA and to equilibrium dissociation constants. It is obvious that the amount of ligand required to observe half of the protein in the free form will greatly depend on actual concentrations of ligand and RNA. Thus, it will be potent under relatively narrow set of conditions (see paper for discussion).

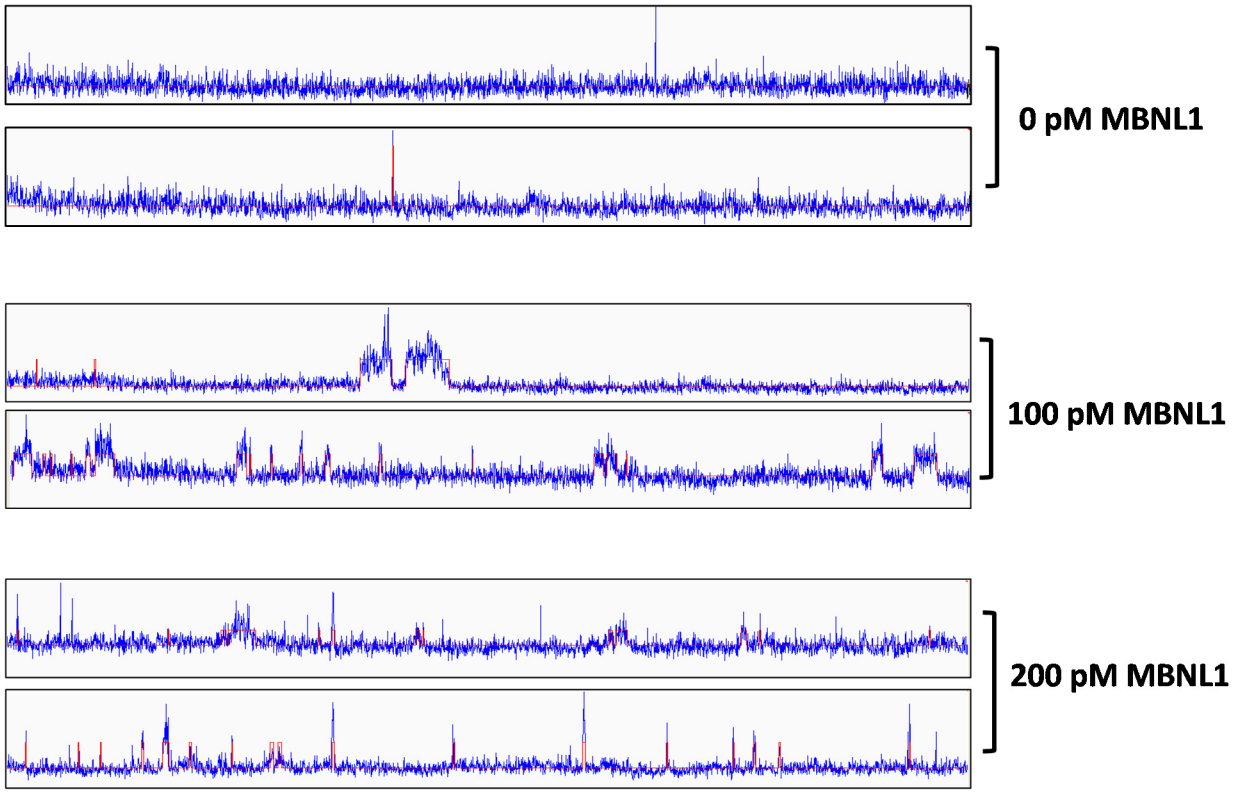

Supplementary Figure S4. Representative trajectories with two-state fitting. Single-molecule trajectories were fit using QuB to reveal the binding and dissociation of MBNL1 to $(CUG)_4$. The data was collected in the standard buffer in the presence of 0 pM, 100 pM and 200 pM MBNL and were globally fit by HMM using QuB software. For representative trajectories fit idealized states (red line) are shown superimposed on the actual Cy3 intensity trajectories (light blue). The trajectories in which $(CUG)_4$ molecules showed either abnormally high Cy5 intensity or more than two-step bleaching were omitted from analysis.

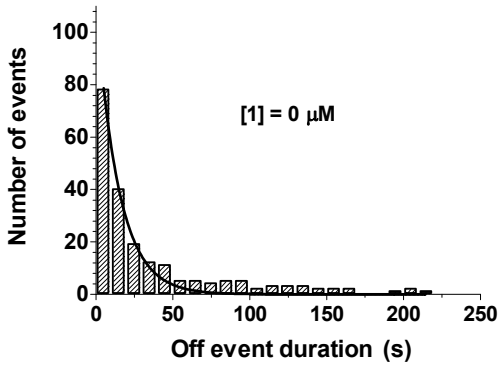

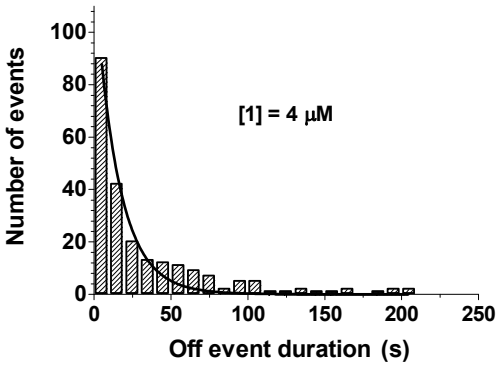

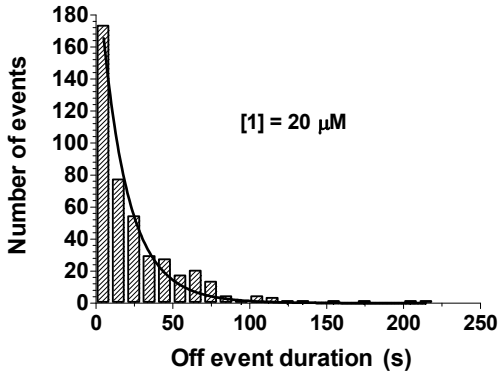

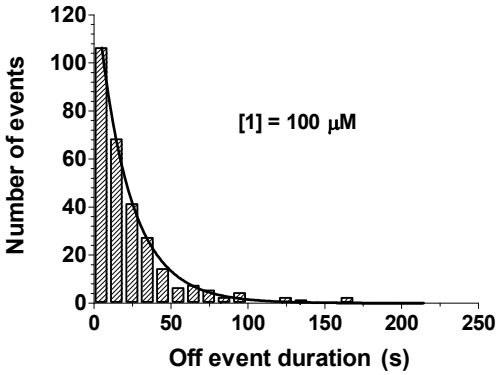

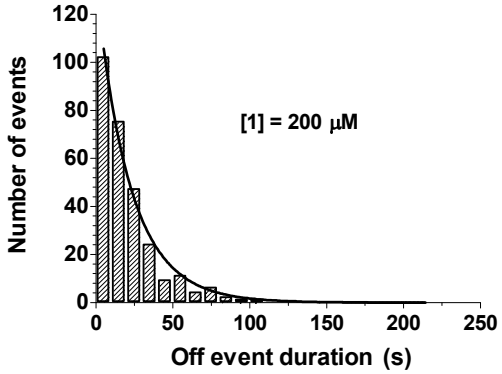

$$Y = Const * \left[K_{d2} * \exp(-k_{+1} * P * t) + [I] * \exp(-k_{+3} * P * t)\right]$$

$K_{d2} = 35.3 \pm 17.3 \mu\text{M}$

$\text{P} = 150\text{pM}$

$k_{+3} = (2.81 \pm 0.19)\text{x}10^{8} s^{-1} M^{-1}$

Supplementary Figure S5. Analysis of the off-event dwell time for different concentrations of **1**. Individual historgams are shown with their respective fitting curves from the global analysis. The equation used to fit the data and the values of obtained variables are shown in the inset.

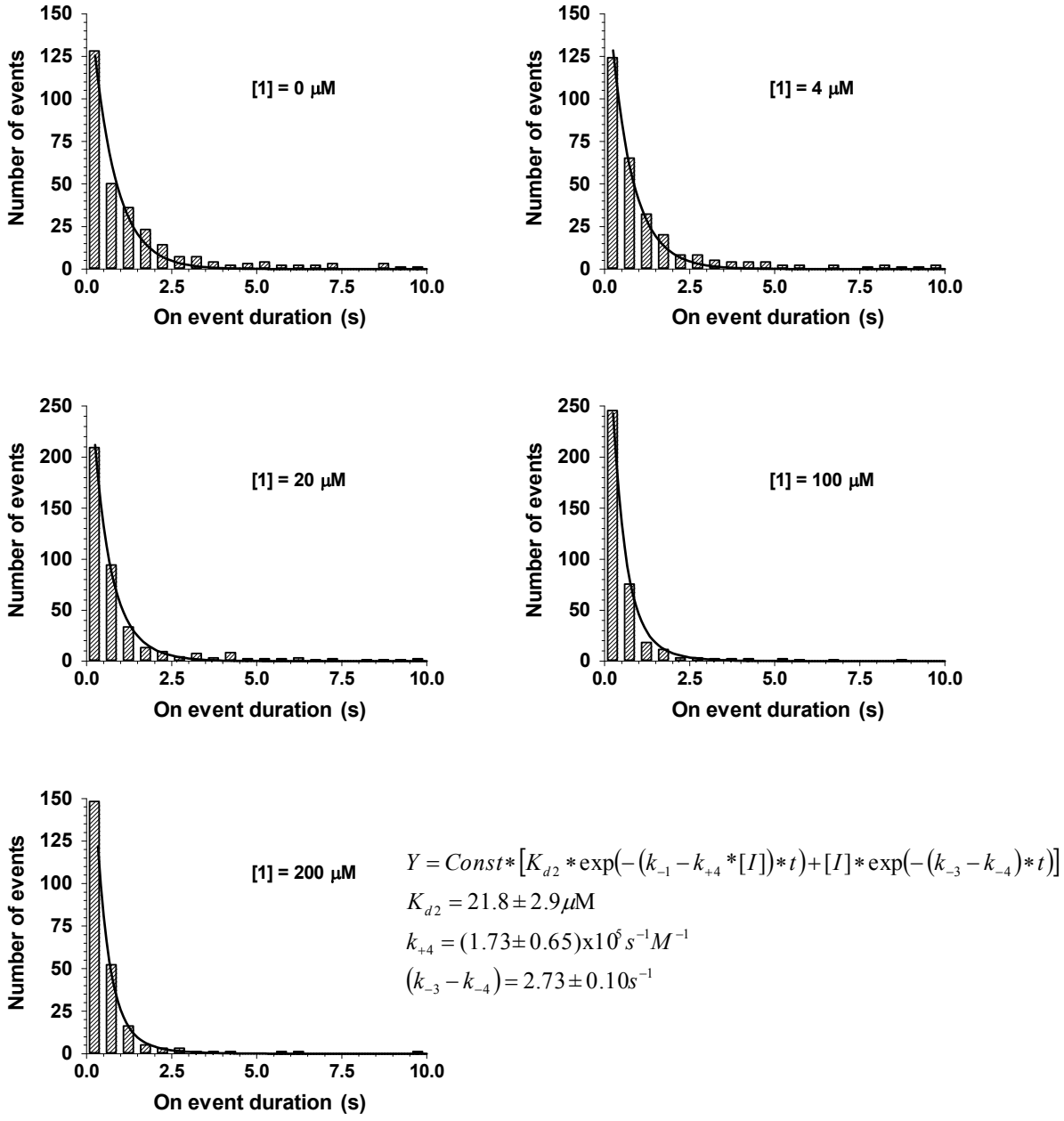

$$Y = Const * \left[K_{d2} * \exp\left(-\left(k_{-1} - k_{+4} * [I]\right) * t\right) + [I] * \exp\left(-\left(k_{-3} - k_{-4}\right) * t\right)\right]$$

$$K_{d2} = 21.8 \pm 2.9 \mu\text{M}$$

$$k_{+4} = (1.73 \pm 0.65)\text{x}10^{5} s^{-1} M^{-1}$$

$$\left(k_{-3} - k_{-4}\right) = 2.73 \pm 0.10 s^{-1}$$

Supplementary Figure S6. Analysis of the on-event dwell time for different concentrations of **1**. Individual historgams are shown with their respective fitting curves from the global analysis. The equation used to fit the data and the values of obtained variables are shown in the inset.

$$Y = Const * \left[K_{d2} * \exp(-k_{+1} * P * t) + [I] * \exp(-k_{+3} * P * t)\right]$$

$K_{d2} = 0.54 \pm 0.39 \mu\text{M}$

$\text{P} = 150\text{pM}$

$k_{+3} = (2.71 \pm 0.16)\text{x}10^{8} s^{-1} M^{-1}$

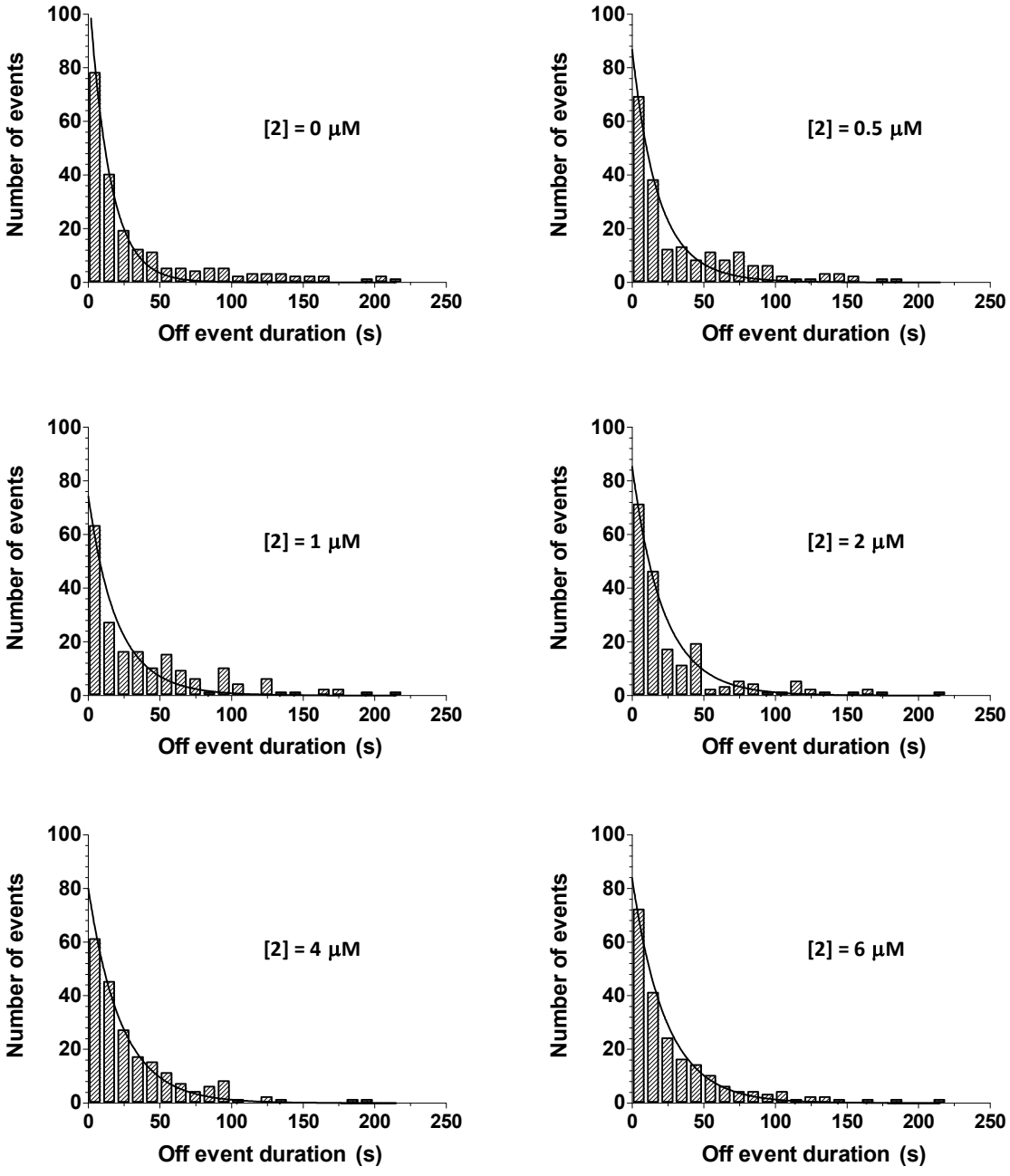

Supplementary Figure S7. Analysis of the off-event dwell time for different concentrations of **2**. Individual historgams are shown with their respective fitting curves from the global analysis. The equation used to fit the data and the values of obtained variables are shown in the inset above.

$$Y = Const * \left[K_{d2} * \exp\left(-\left(k_{-1} - k_{+4} * [I]\right) * t\right) + [I] * \exp\left(-\left(k_{-3} - k_{-4}\right) * t\right)\right]$$

$$K_{d2} = 0.45 \pm 0.02 \mu\text{M}$$

$$k_{+4} = (1.93 \pm 0.03)\text{x}10^{6} s^{-1} M^{-1}$$

$$\left(k_{-3} - k_{-4}\right) = 4.85 \pm 0.26 s^{-1}$$

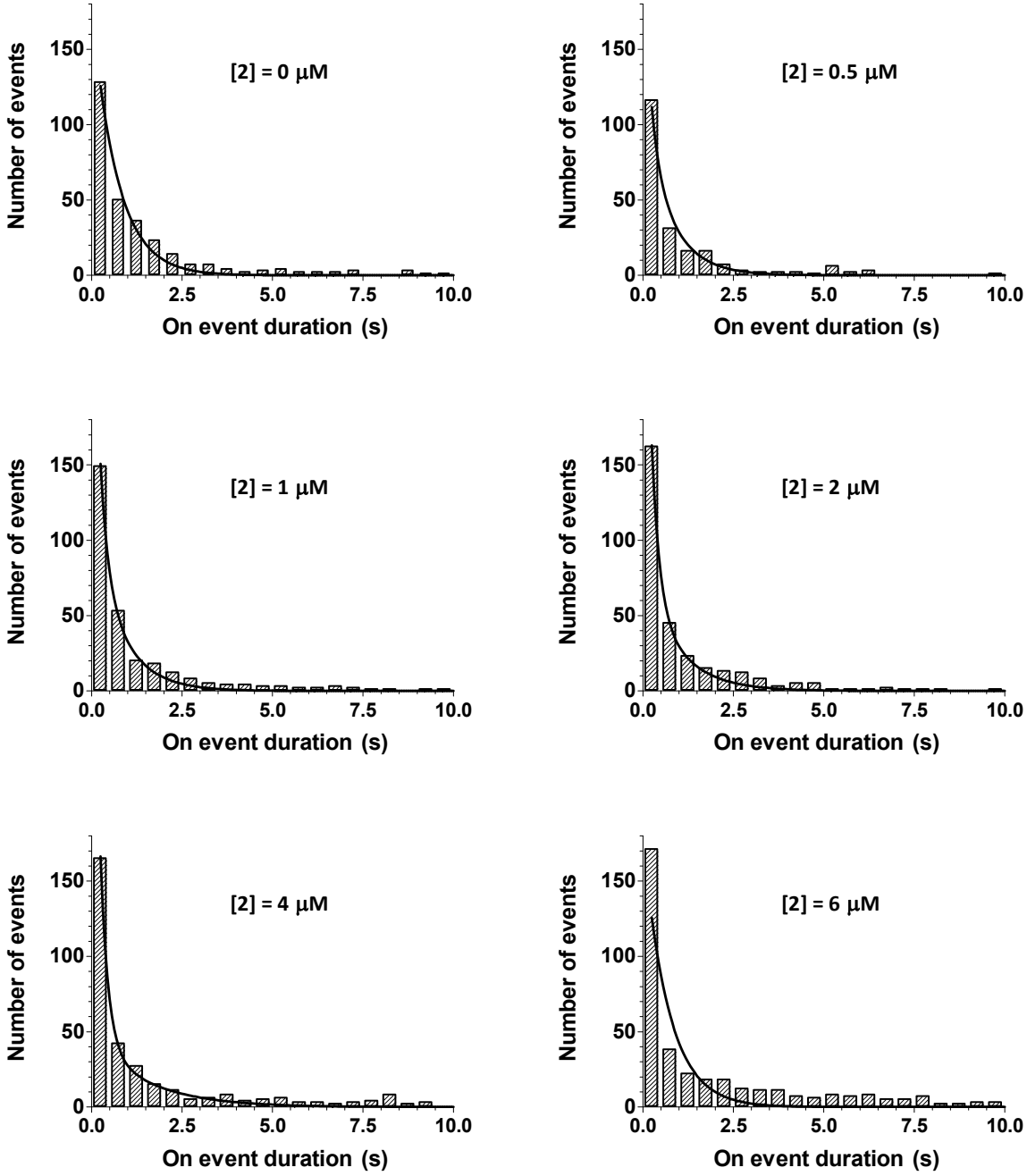

Supplementary Figure S8. Analysis of the on-event dwell time for different concentrations of **2**. Individual historgams are shown with their respective fitting curves from the global analysis. The equation used to fit the data and the values of obtained variables are shown in the inset above.

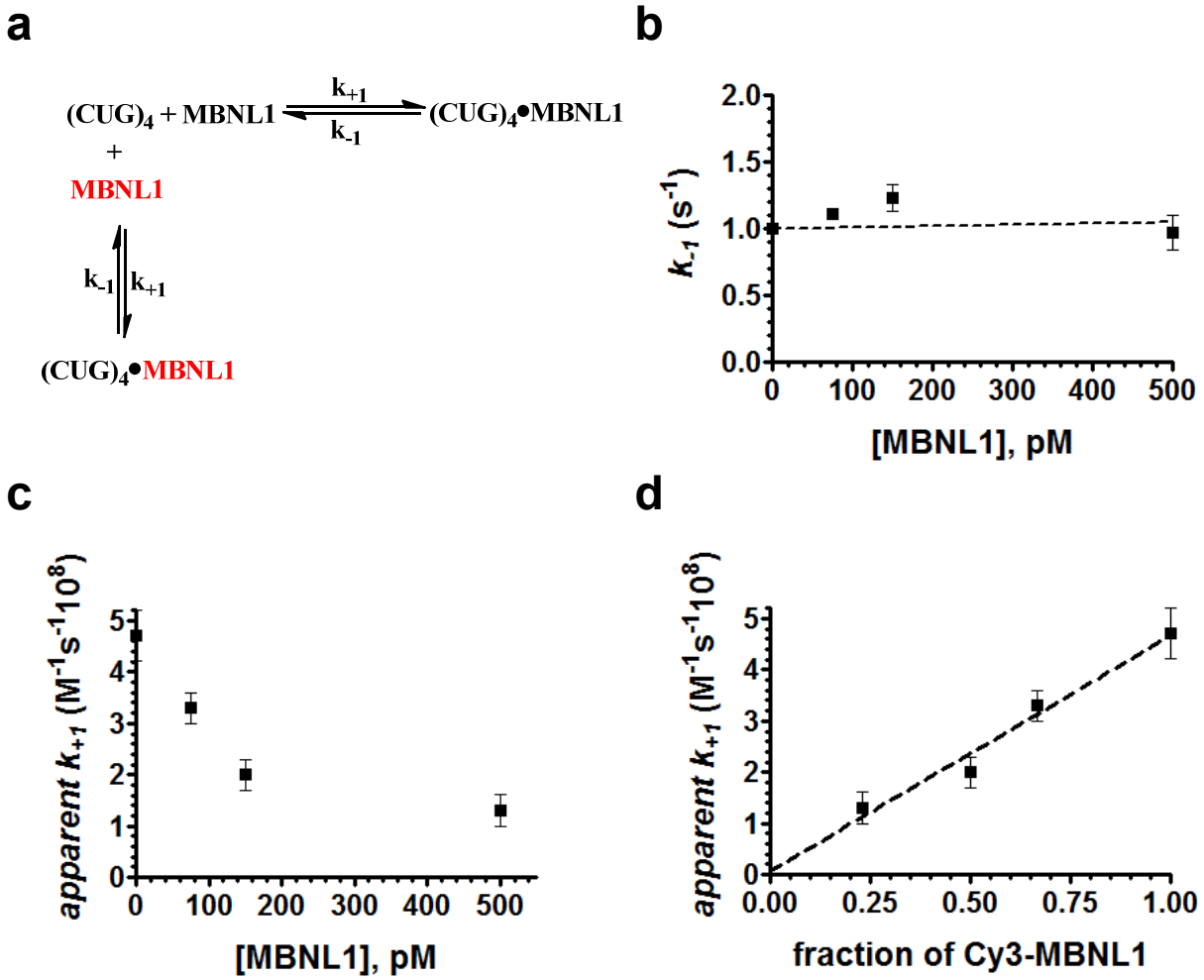

Supplementary Figure S9. Unlabeled MBNL1 acts as a competitive inhibitor. (**a**) Schematic representation of competitive inhibition. (**b** and **c**) k_{-1} is unaffected by addition of unlabeled MBNL1 whereas apparent k_{+1} is decreased. (**d**) k_{+1} is linearly dependent on [Cy3-MBNL1]/ ([unlabeled MBNL1] +[Cy3-MBNL1]) ratio.

Supplementary Note 3

To provide independent support for the single-molecule TIRF microscopy method, we used SPR to study the inhibition of MBNL1 binding to $(CUG)_4$ and $(CUG)_{12}$. Biotinylated RNA constructs were immobilized on a streptavidin coated surface. The immobilization density for most of the experiments was kept under 100 RU. For the stoichiometry study of MBNL1 binding to $(CUG)_{12}$, 1100 RU of $(CUG)_{12}$ was immobilized. Stoichiometry of MBNL1 binding to CUG12 was obtained by measuring the steady state binding response from the injection of a highly concentrated MBNL1 solution (12 μM) for 120 s. Although the RU is still not fully reached the maximum steady state, we could approximately derive the stoichiometry ratio for MBNL1 binding to $(CUG)_{12}$ using this equation: $R_L = (\frac{R_{max}}{S_m})(\frac{MW_L}{MW_A})$

R_L is the density of immobilized $(CUG)_{12}$, ligand, on the chip surface; R_{max} is the maximum binding response for MBNL1 binding; S_m is the binding stoichiometry; MW_L is the molecular weight of $(CUG)_{12}$, 13293 Da, and MW_A is the molecular weight of GST-MBNL1 analyte, 60489 Da.

Analysis of the steady-state SPR response unit (RU) yielded a binding stoichiometry of almost 3:1 for MBNL1 binding to $(CUG)_{12}$, which implies that one $(CUG)_{12}$ can bind to three MBNL1 proteins.

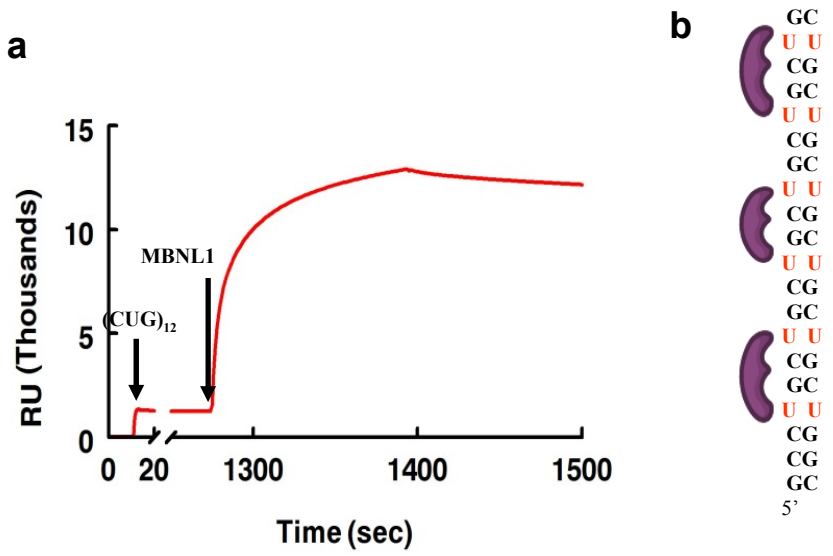

Supplementary Figure S10. Representative sensogram for stoichiometric study of MBNL1·$(CUG)_{12}$ interaction. (**a**) The arrows show the starting point of $(CUG)_{12}$ immobilization and MBNL1 injection. The sensogram suggests stoichiometric ratio of 3:1 for MBNL1:$(CUG)_{12}$ binding as shown schematically in (**b**).

RU change in the sensogram was observed upon addition of inhibitors **1** and **2** as well as MBNL1, indicating binding to the biotinylated CUG repeats. Therefore, for the inhibition studies at different concentrations of small molecules, simultaneous injection of both MBNL1 and inhibitors made the analysis impossible. This limitation results from the fact that the RU signal would have to be deconvoluted to determine whether the binding is from MBNL1 or the small molecule. To circumvent this problem, we set up an experiment in which injection of the small molecule preceded the injection of MBNL1. This way, by pre-incubation of the surface with small molecule, we were able to reach the plateau binding level of the small molecule. Then, while keeping the small molecule concentration the same, the second injection gave rise only to the MBNL1 binding. With the assumption that ligand does not dissociate significantly under these conditions, the proportion of MBNL1 binding that is inhibited at any concentration of small molecule could be determined. The highest RU was measured at the point that the injection was stopped. This is end point of the association phase and start of the dissociation phase. This RU is an indication of MBNL1 binding level, therefore the higher the inhibitor concentration, the lower this would be point.

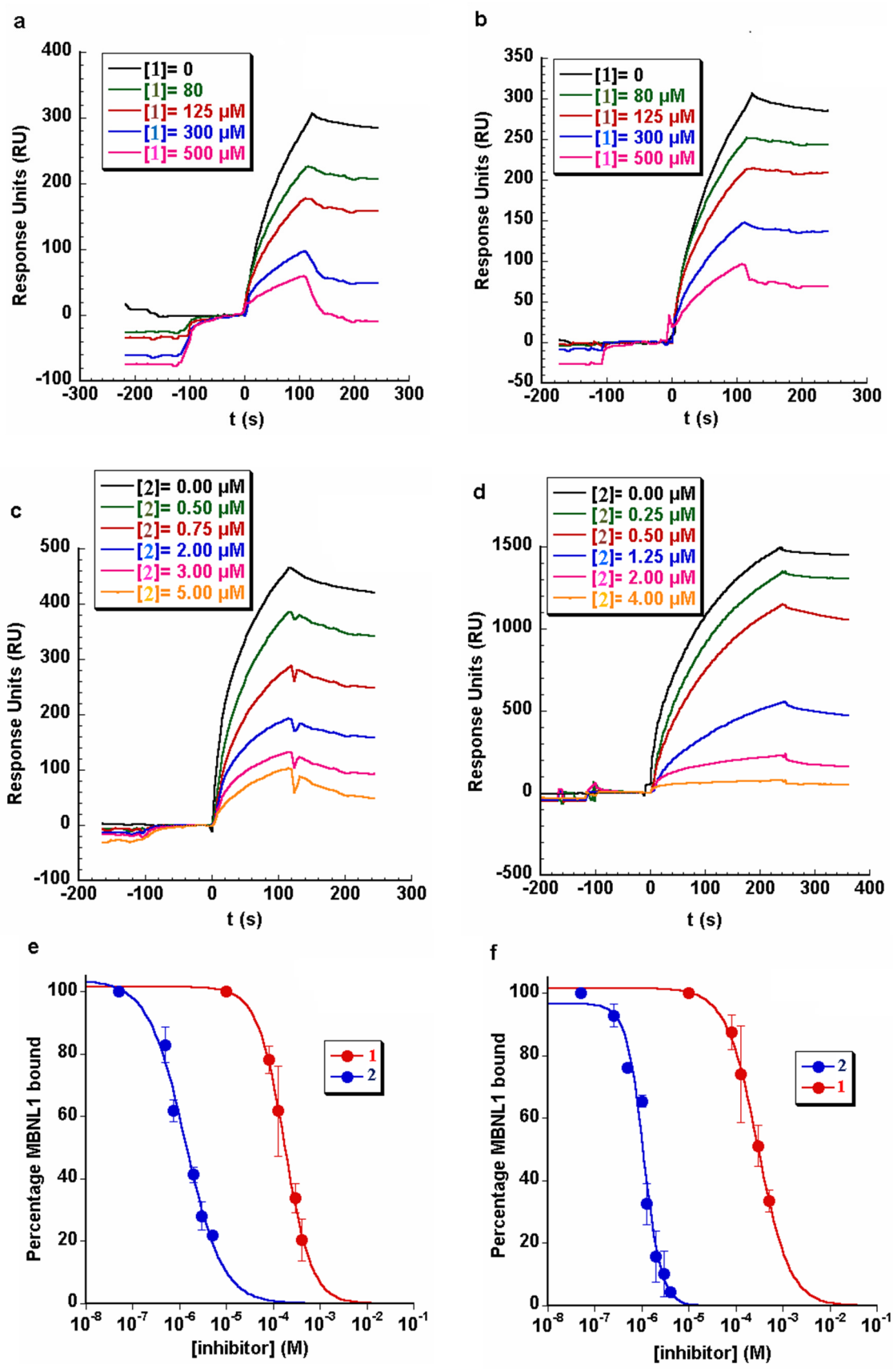
a
[1]= 0
[1]= 80
[1]= 125 µM
[1]= 300 µM
[1]= 500 µM
Response Units (RU)
t (s)
b
[1]= 0
[1]= 80 µM
[1]= 125 µM
[1]= 300 µM
[1]= 500 µM
Response Units (RU)
t (s)
c
[2]= 0.00 µM
[2]= 0.50 µM
[2]= 0.75 µM
[2]= 2.00 µM
[2]= 3.00 µM
[2]= 5.00 µM
Response Units (RU)
t (s)
d
[2]= 0.00 µM
[2]= 0.25 µM
[2]= 0.50 µM
[2]= 1.25 µM
[2]= 2.00 µM
[2]= 4.00 µM
Response Units (RU)
t (s)
e
Percentage MBNL1 bound
1
2
[inhibitor] (M)
f
Percentage MBNL1 bound
2
1
[inhibitor] (M)

Supplementary Figure S11. Representative Sensograms from SPR studies and fitting data to dose-response curves. Biotinylated $(CUG)_4$ is the immobilized ligand in (**a**) and (**c**). Biotinylated $(CUG)_{12}$ is the immobilized ligand in (**b**) and (**d**). Varying concentration of **1** and **2** are injected from t = -120 s to either t = 120 s (**a**, **b** and **c**) or t = 240 s (**d**). GST-MBNL1, 0.65 μM, is injected from t = 0 s to either t = 120 s (**a**, **b** and **c**) or t = 240 s (**d**). Baseline for the curves was set to RU = 0 at t = 0. (**e**) Inhibition of MBNL1 binding to $(CUG)_4$ in the presence of varying concentrations of **1** and **2**. (**f**) Inhibition of MBNL1 binding to $(CUG)_{12}$ in the presence of varying concentrations of **1** and **2**. Error bars represent mean ± s.d. of three replicates.

For each ligand the fact that apparent IC_{50} values for inhibition of MBNL1 binding to either $(CUG)_4$ and $(CUG)_{12}$ are close, supports the previous findings that both these constructs are acceptable models for CUG repeat (6). Normalized IC_{50} values can be calculated by multiplying the actual IC_{50} by the number of binding modules it has. The ratio between normalized IC_{50} values is the bivalent effect, which is almost 120-fold for **2**. This improvement in inhibition confirms the inhibition result obtained by single molecule TIRF microscopy, however, by this method, we were unable to measure how the binding kinetic change in the presence of inhibitors or reveal the inhibition mode of the ligands. This is due to the fact that this technique doesn't allow us to differentiate binding of inhibitor from MBNL1. Therefore at any concentration of inhibitor, whether in association or dissociation phase, we are detecting association and dissociation of both MBNL1 and small molecules to the immobilized RNA construct. This deficiency is overcome in the single molecular TIRFM experiments by only MBNL1 with Cy3 which enables us to detect binding and unbinding of an individual MBNL1 protein.

Supplementary Note 4

To verify that **1** and **2** don't bind to MBNL1 protein we carried out Isothermal titration calorimetry experiments. ITC titration curves show no measureable interaction between the ligands and MBNL1 protein.

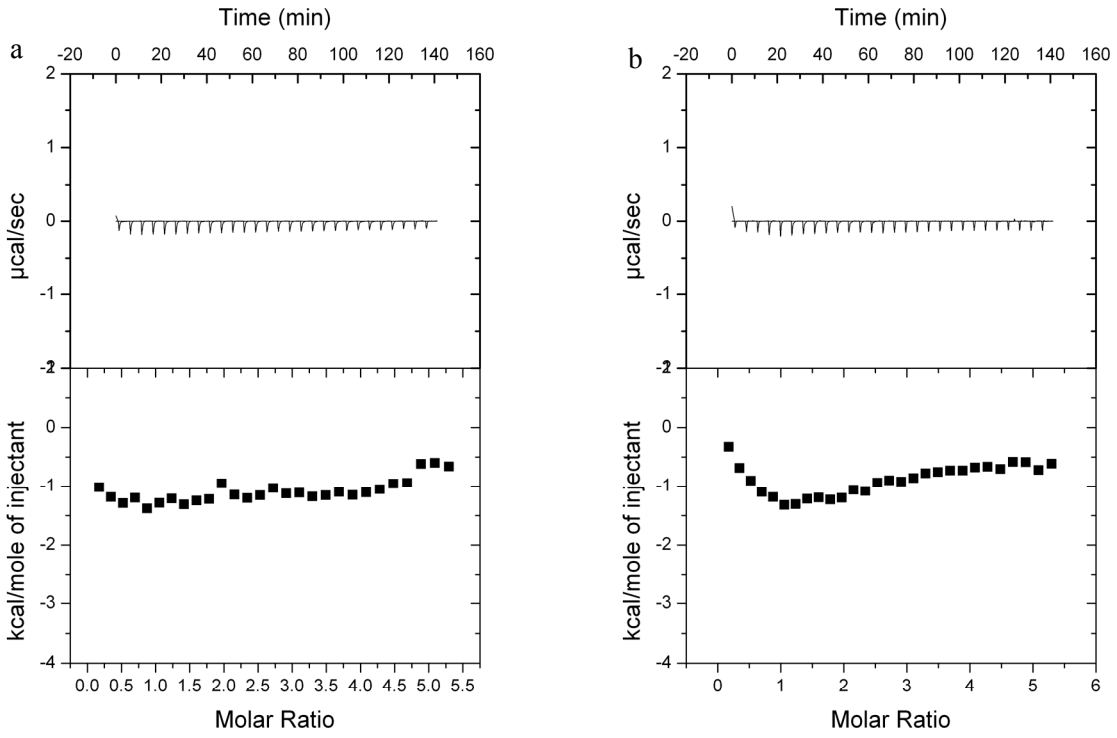

Supplementary Figure S12. ITC binding isotherms and titration curves of **1** (a) and **2** (b) to MBNL1.solution. No measureable binding is observed.

Supplementary Note 5

The sequences and modifications for all RNA constructs used in this study:

$(CUG)_4$ construct for SPR studies:

5'- GCUGCUGUUCGCUGCUG-TEG-Biotin - 3'

$(CUG)_4$ construct for TIRF studies:

5'- Cy5-GCUGCUGUUCGCUGCUG-TEG-Biotin – 3'

$(CUG)_6$ construct for fluorescence binding studies:

5'- TAMRA-CUGCUGCUGCUGCUGCUG – 3'

$(CUG)_{12}$ construct for TIRF and SPR experiments:

5'- GCCUGCUGCUGCUGCUGCUGCUGCUGCUGCUGCUGCUGGC-TEG-Biotin – 3'

Supplementary Methods

Surface Plasmon Resonance (SPR) Analysis

All SPR experiments were conducted on a streptavidin coated sensor chip using a Biacore 3000 instrument. Streptavidin coated research grade sensor chips were preconditioned with three consecutive 1-minute injections of 1 M NaCl/ 50 mM NaOH before the immobilization was started. 3'-biotin labeled RNA (CUG_4 or CUG_{12}) was captured on flow cell 2 (Response Unit, RU, between 100-1100). Flow cell 1 was used as a reference. Inhibition analysis was carried out in PBS, 1X buffer, pH = 7.4, containing 0.05% Tween-20 and 0.2 mg/mL (7.4 μM or 580 μM nucleotides) bulk yeast t-RNA to confirm the specificity of inhibition. Various concentrations of **1** and **2** were flowed at a rate of 20 μL/min for 240 s over the immobilized RNA. After the initial 120 s, a solution of GST-MBNL1 protein, 600 nM, in the same buffer was also flowed over the surface for the rest of time, 120 s. The reference-subtracted sensograms were recorded.

After the dissociation phase, the surface was regenerated, with a pulse of 0.5% SDS and/or 100 mM NaOH, for a few times followed by buffer wash to re-establish baseline. RU upon the injection of PBS buffer was subtracted from sensograms. For inhibition studies, the resulting sensograms were baselined at t = 120 s to offset the binding of small molecule to the immobilized RNA surface. The peak RU (t = 120 s) was recorded. Two or three separate SPR experiments on different sensor chips with different levels of RNA immobilization were performed to verify that the values are not affected by surface RNA density.

Isothermal Titration Calorimetry

ITC measurements were performed at 25 °C on a MicroCal VP-ITC (MicroCal). Experiment consisted of titrating 10 μL of a 5 μM ligand from a 280 μL syringe (rotating at 300 rpm), for a total of 28 injections, into a sample cell containing 1.42 mL of a 0.2 μM MBNL1N solution. The duration of the injection was set to 24 s, and the delay between injections was 300 s. The initial delay before the first injection was 60 s. To derive the heat associated with each injection, the area under each isotherm (microcalories per second versus seconds) was determined by integration by the graphing program Origin 5.0 (MicroCal). The stock solution of **1** and **2** were 10mM in DMSO and water, respectively. The buffer solution for ITC experiments was 1X PBS, pH 7.0. 5% DMSO was added to the buffer for experiments with **1** to balance the residual DMSO in the ligand solution.

Supplementary References

1. Arambula, J.F., Ramisetty, S.R., Baranger, A.M. and Zimmerman, S.C. (2009) A simple ligand that selectively targets CUG trinucleotide repeats and inhibits MBNL protein binding. *Proc. Natl. Acad. Sci. U. S. A.*, **106**, 16068-16073.

2. Mei, X., August, A.T. and Wolf, C. (2006) Regioselective copper-catalyzed amination of chlorobenzoic acids: synthesis and solid-state structures of N-aryl anthranilic acid derivatives. *J. Org. Chem.*, **71**, 142-149.

3. Kauffman, M. (1990) 4-(2-Carboxyphenyl)aminobenzenealkanoic. *J. Pharm. Sci.*, **79**, 173-178.

4. Ilies, M.A., Seitz, W.a., Johnson, B.H., Ezell, E.L., Miller, A.L., Thompson, E.B. and Balaban, A.T. (2006) Lipophilic pyrylium salts in the synthesis of efficient pyridinium-based cationic lipids, gemini surfactants, and lipophilic oligomers for gene delivery. *J. Med. Chem.*, **49**, 3872-3887.

5. Cuenca, F., Moore, M.J., Johnson, K., Guyen, B., De Cian, A. and Neidle, S. (2009) Design, synthesis and evaluation of 4,5-di-substituted acridone ligands with high G-quadruplex affinity and selectivity, together with low toxicity to normal cells. *Bioorg. Med. Chem. Lett.*, **19**, 5109-5113.

6. Warf, M.B. and Berglund, J.A. (2007) MBNL binds similar RNA structures in the CUG repeats of myotonic dystrophy and its pre-mRNA substrate cardiac troponin T. *RNA*, **13**, 2238-2251.

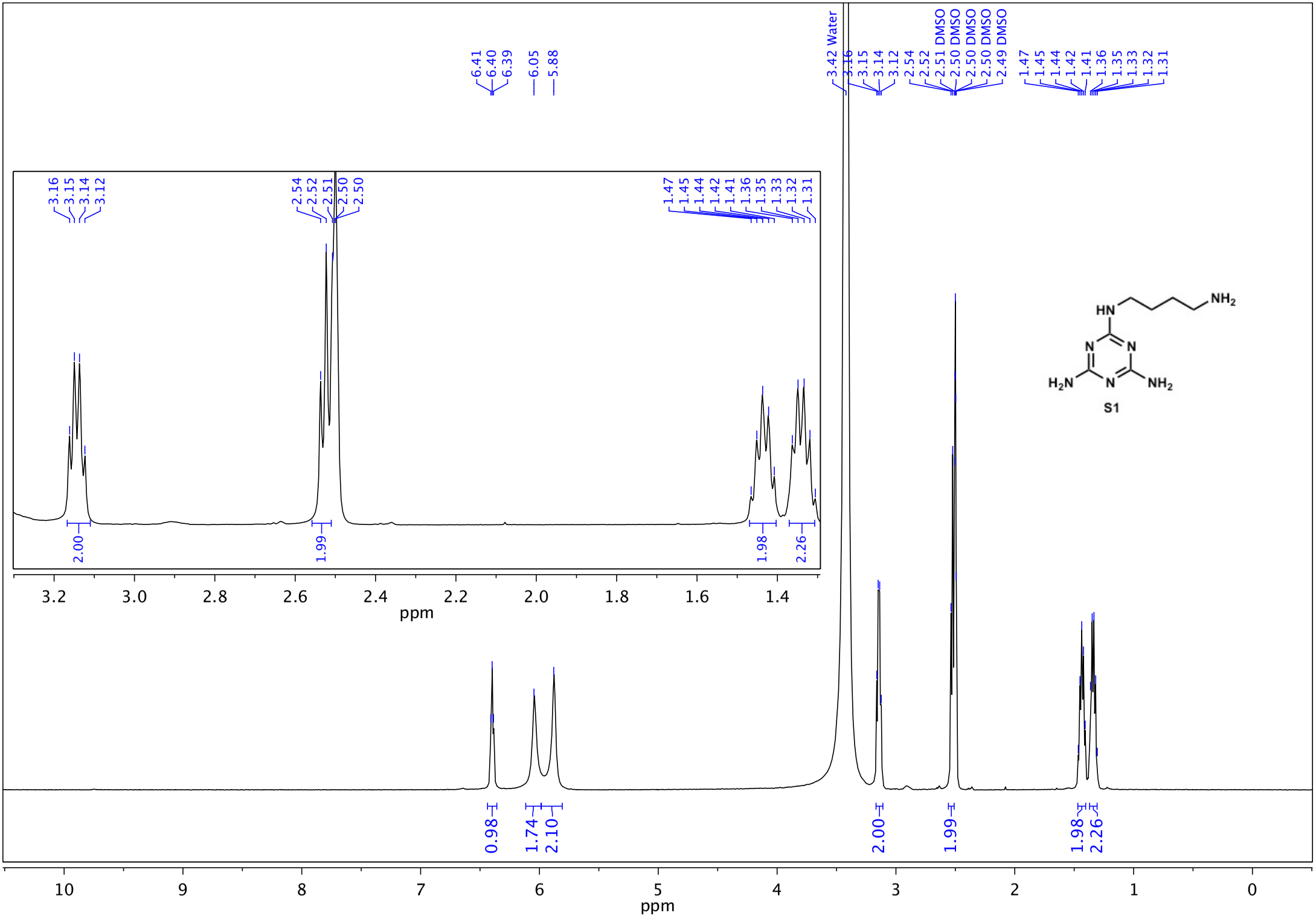
6.41
6.40
6.39
6.05
5.88
3.42 Water
3.16
3.15
3.14
3.12
2.54
2.52
2.51 DMSO
2.50 DMSO
2.50 DMSO
2.50 DMSO
2.49 DMSO
1.47
1.45
1.44
1.42
1.41
1.36
1.35
1.33
1.32
1.31
HN
NH2
N
N
H2N
N
NH2
S1
0.98
1.74
2.10
2.00
1.99
1.98
2.26
ppm
ppm

9.87
7.95
7.93
7.88
7.86
7.49
7.47
7.28
7.26
6.96
6.95
6.95
6.94
6.94
6.93
6.93
6.93
6.92
7.95
7.93
7.88
7.86
7.50
7.49
7.47
7.46
7.28
7.26
6.96
6.95
6.95
6.94
6.94
6.93
6.93
6.93
6.92
1.00
2.01
2.09
1.82
0.93
0.02
0.03
0.06
0.03
0.07
0.07
0.03
1.71
3.41 Water
2.51 DMSO
2.50 DMSO
2.50 DMSO
2.50 DMSO
2.49 DMSO
S2
ppm
ppm

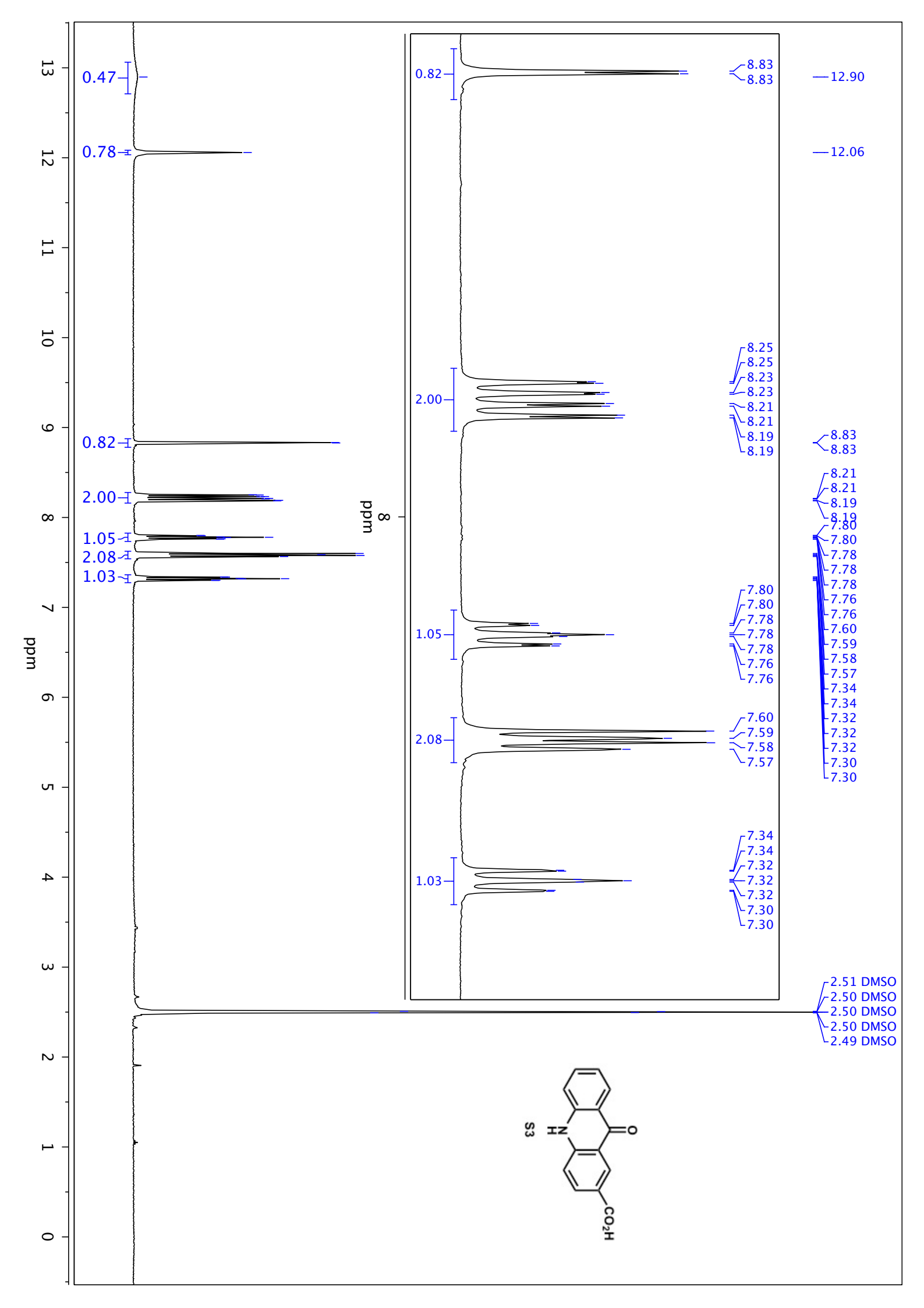
0.47
0.78
0.82
2.00
1.05
2.08
1.03
ppm
0.82
2.00
1.05
2.08
1.03
8.83
8.83
8.25
8.25
8.23
8.23
8.21
8.21
8.19
8.19
7.80
7.80
7.78
7.78
7.78
7.76
7.76
7.60
7.59
7.58
7.57
7.34
7.34
7.32
7.32
7.32
7.30
7.30
12.90
12.06
8.83
8.83
8.21
8.21
8.19
8.19
7.80
7.80
7.78
7.78
7.78
7.76
7.76
7.60
7.59
7.58
7.57
7.34
7.34
7.32
7.32
7.32
7.30
7.30
2.51 DMSO
2.50 DMSO
2.50 DMSO
2.50 DMSO
2.49 DMSO
S3
N
H
O
CO2H

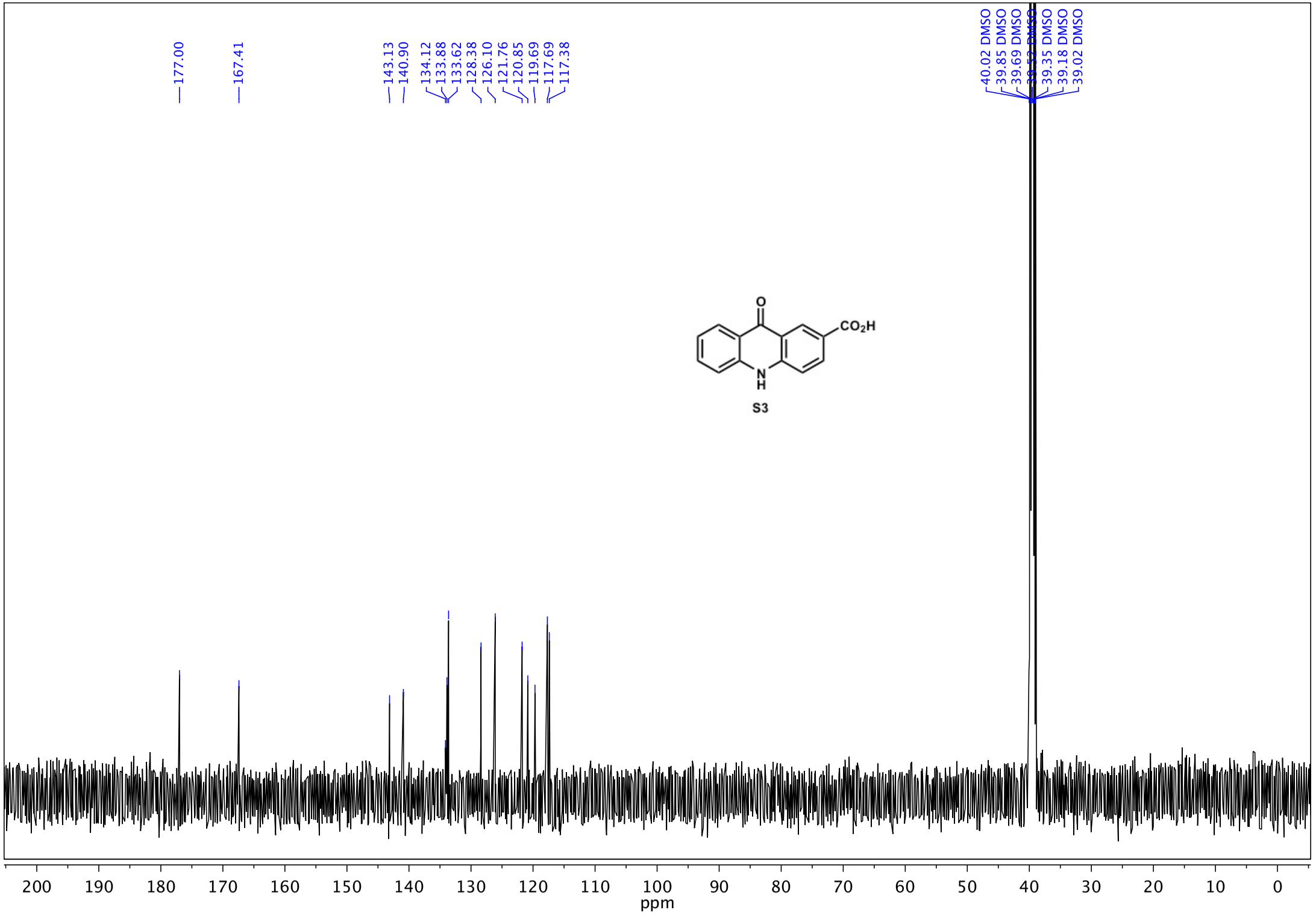
177.00
167.41
143.13
140.90
134.12
133.88
133.62
128.38
126.10
121.76
120.85
119.69
117.69
117.38
40.02 DMSO
39.85 DMSO
39.69 DMSO
39.52 DMSO
39.35 DMSO
39.18 DMSO
39.02 DMSO
O
CO2H
N
H
S3
200
190
180
170
160
150
140
130
120
110
100
90
80
70
60
50
40
30
20
10
0
ppm

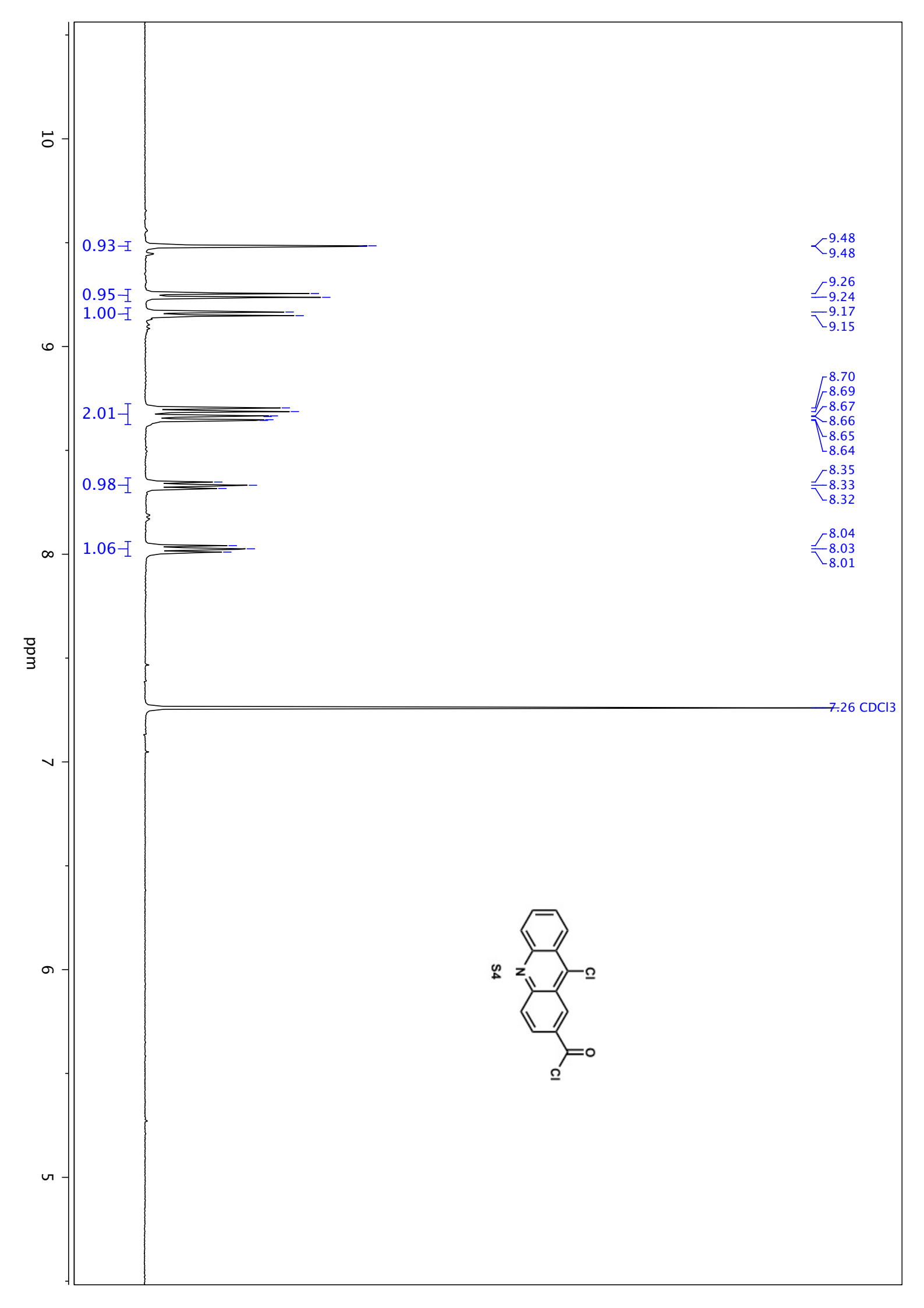
0.93
0.95
1.00
2.01
0.98
1.06
9.48
9.48
9.26
9.24
9.17
9.15
8.70
8.69
8.67
8.66
8.65
8.64
8.35
8.33
8.32
8.04
8.03
8.01
7.26 CDCl3
ppm
10
9
8
7
6
5
S4
N
Cl
O
Cl

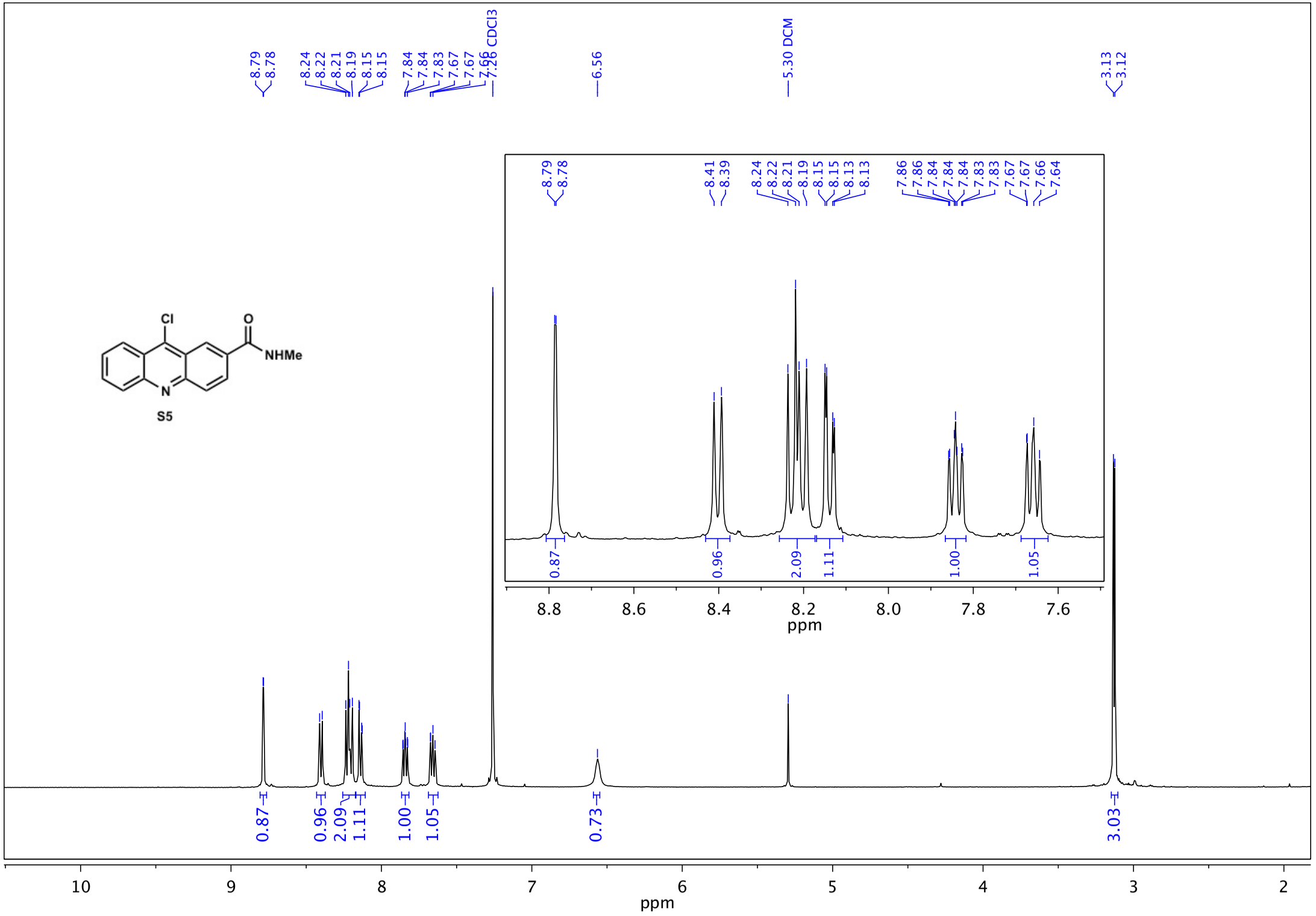
8.79
8.78
8.24
8.22
8.21
8.19
8.15
8.15
7.84
7.84
7.83
7.67
7.67
7.66 CDCl3
6.56
5.30 DCM
3.13
3.12
Cl
O
NHMe
N
S5
8.41
8.39
7.86
7.86
7.84
7.84
7.84
7.83
7.83
7.67
7.67
7.66
7.64
0.87
0.96
2.09
1.11
1.00
1.05
0.73
3.03
ppm

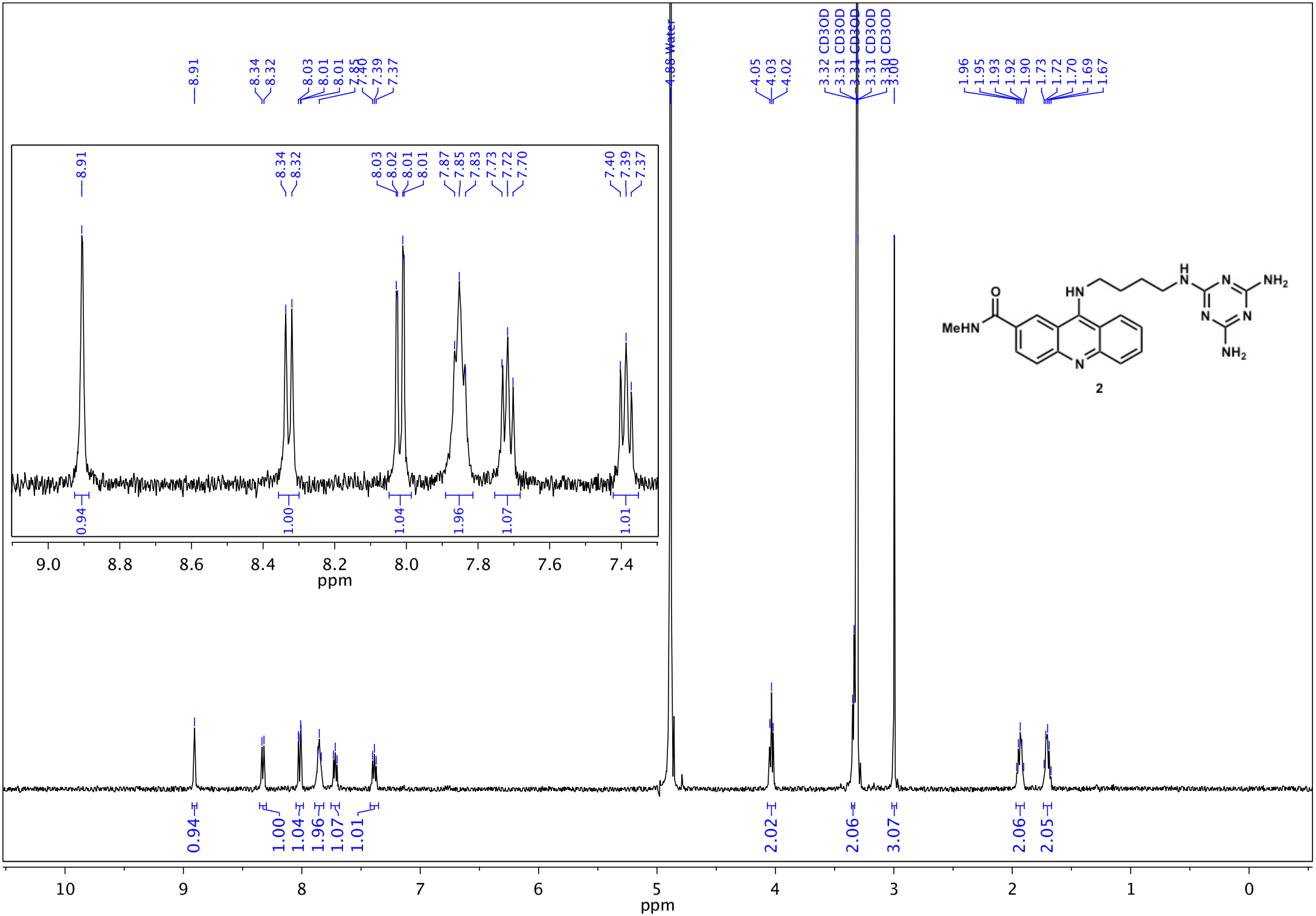
8.91
8.34
8.32
8.03
8.01
8.01
7.85
7.40
7.39
7.37
4.88 Water
4.05
4.03
4.02
3.32 CD3OD
3.31 CD3OD
3.31 CD3OD
3.31 CD3OD
3.30 CD3OD
3.00
1.96
1.95
1.93
1.92
1.90
1.73
1.72
1.70
1.69
1.67
0.94
1.00
1.04
1.96
1.07
1.01
2.02
2.06
3.07
2.06
2.05
ppm
MeHN
HN
NH2
NH2
2

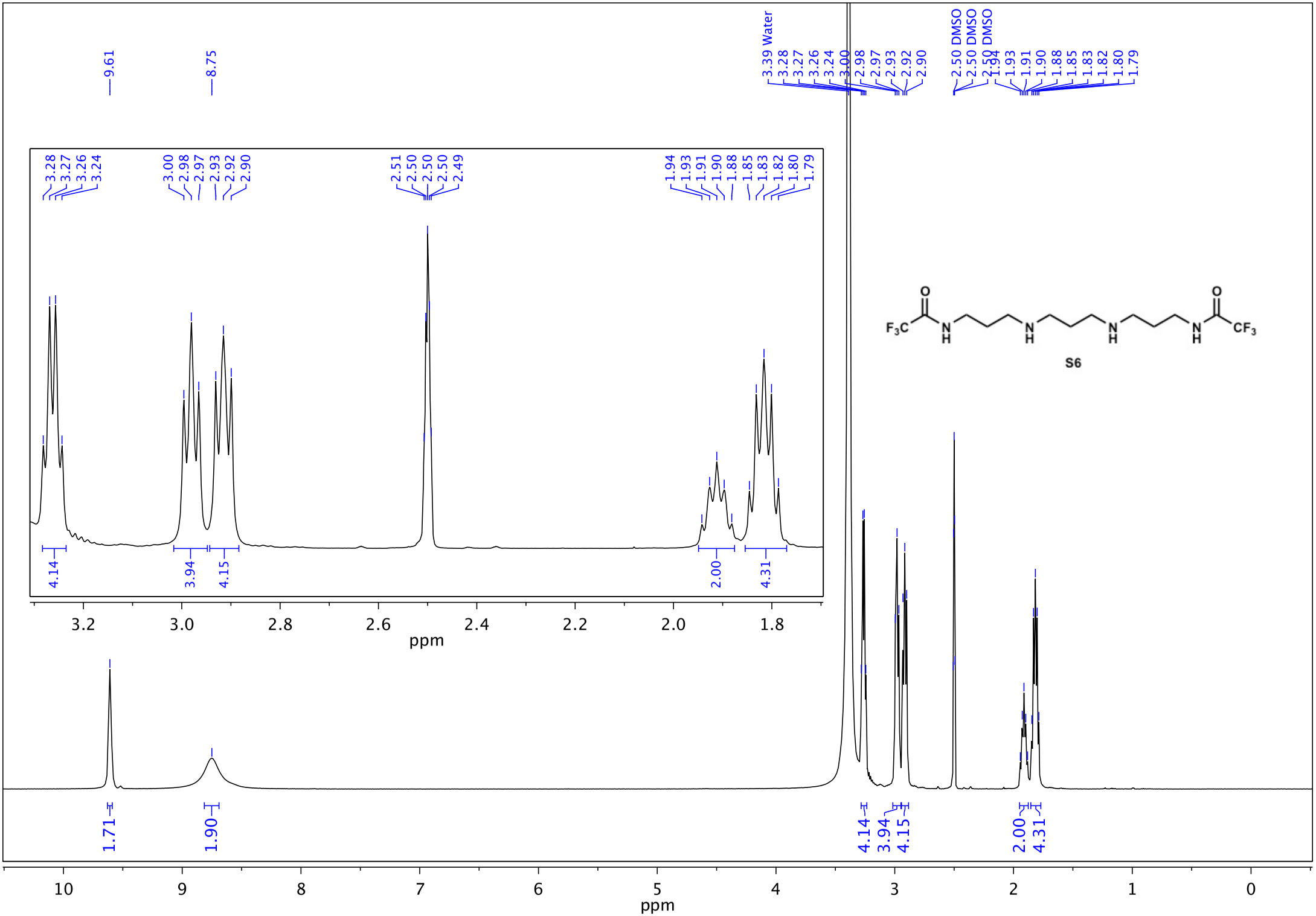
9.61
8.75
3.39 Water
3.28
3.27
3.26
3.24
3.00
2.98
2.97
2.93
2.92
2.90
2.50 DMSO
2.50 DMSO
2.50 DMSO
1.94
1.93
1.91
1.90
1.88
1.85
1.83
1.82
1.80
1.79
2.51
2.50
2.50
2.50
2.49
4.14
3.94
4.15
2.00
4.31
3.2
3.0
2.8
2.6
2.4
2.2
2.0
1.8
ppm
F3C
CF3
S6
1.71
1.90
4.14
3.94
4.15
2.00
4.31
10
9
8
7
6
5
4
3
2
1
0
ppm

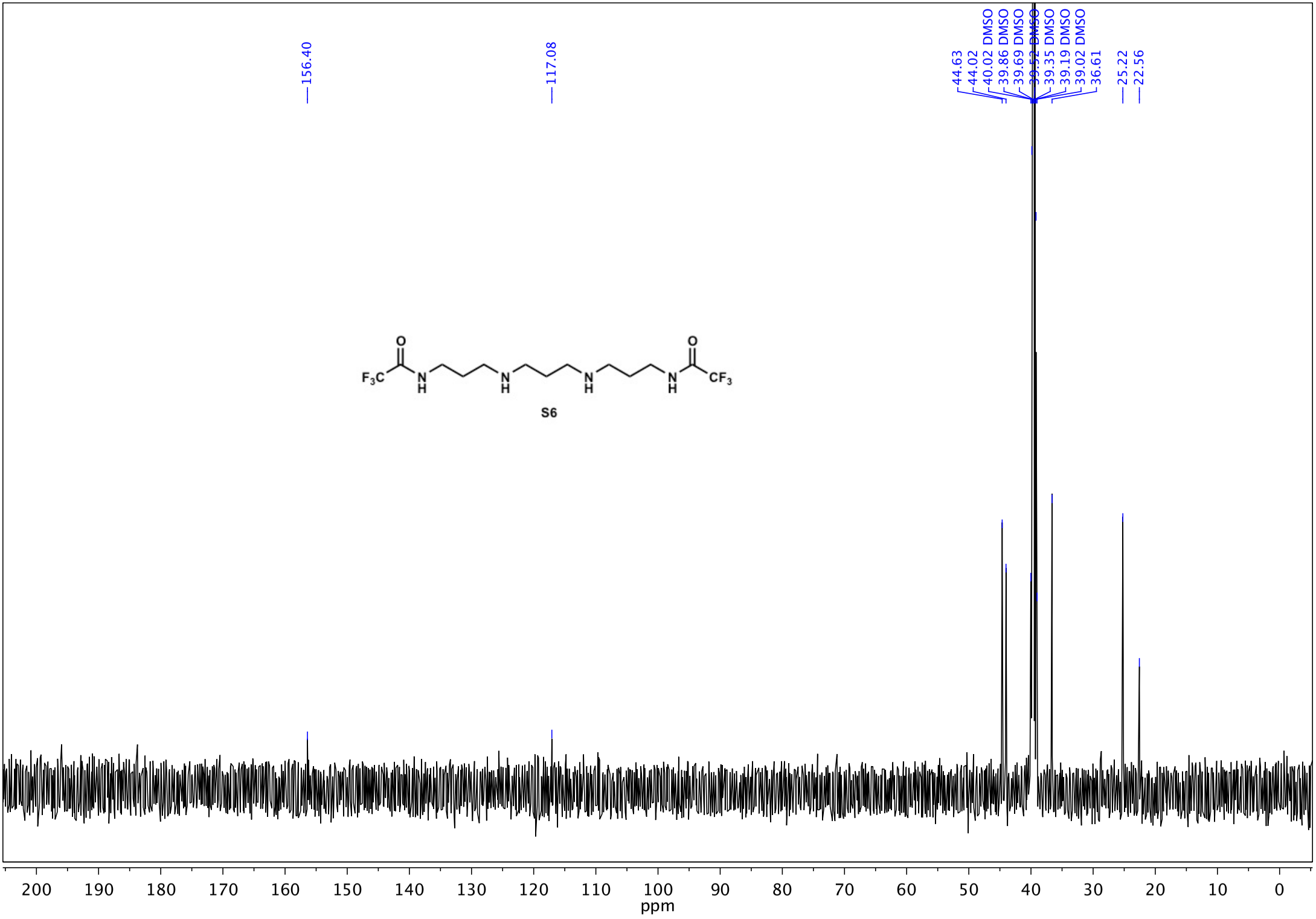
156.40
117.08
44.63
44.02
40.02 DMSO
39.86 DMSO
39.69 DMSO
39.52 DMSO
39.35 DMSO
39.19 DMSO
39.02 DMSO
36.61
25.22
22.56
O
F3C
N
H
N
H
N
H
N
H
O
CF3
S6
200
190
180
170
160
150
140
130
120
110
100
90
80
70
60
50
40
30
20
10
0
ppm

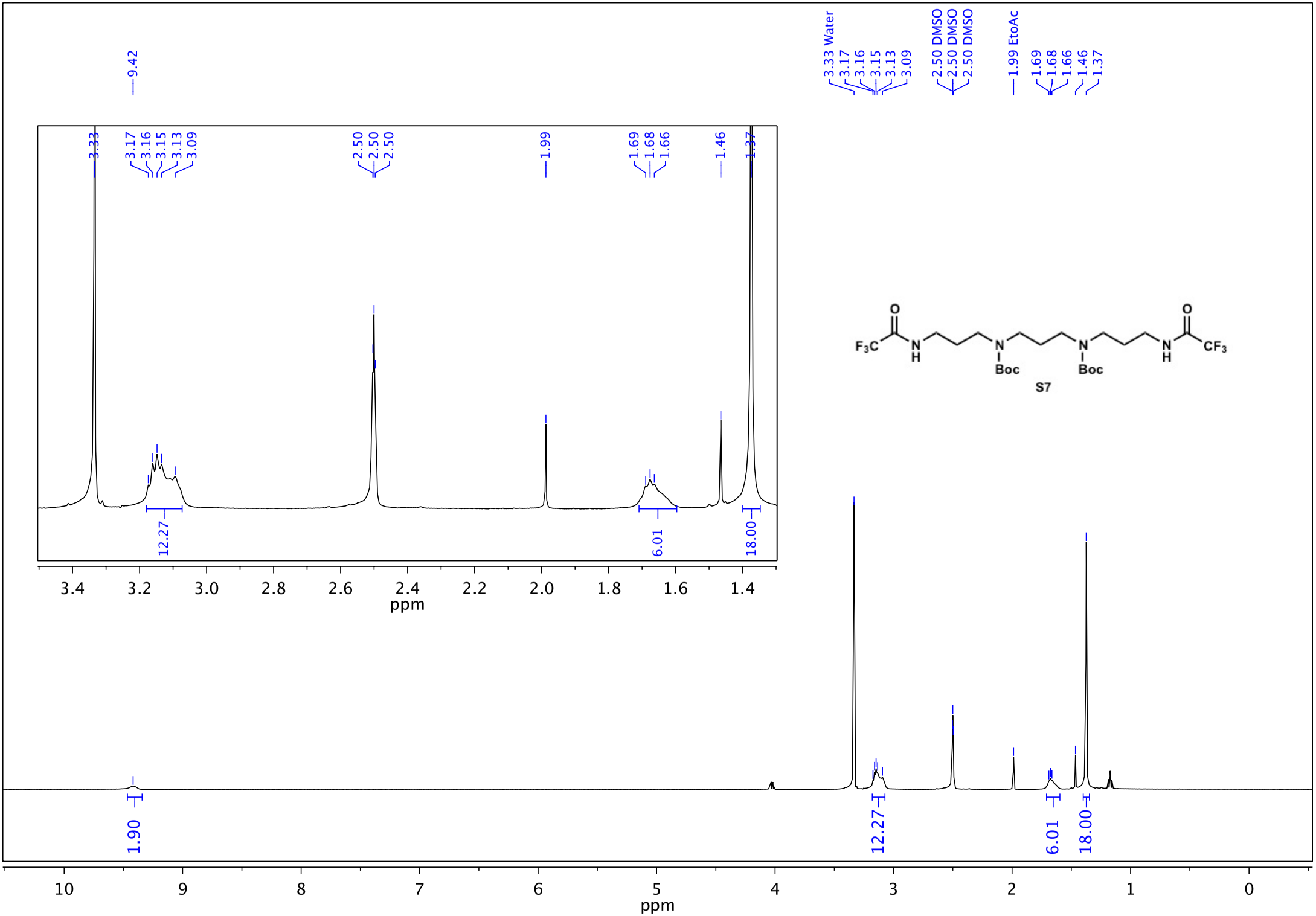
9.42
3.33 Water
3.17
3.16
3.15
3.13
3.09
2.50 DMSO
2.50 DMSO
2.50 DMSO
1.99 EtoAc
1.69
1.68
1.66
1.46
1.37
F3C
CF3
Boc
Boc
S7
1.90
12.27
6.01
18.00
ppm
ppm

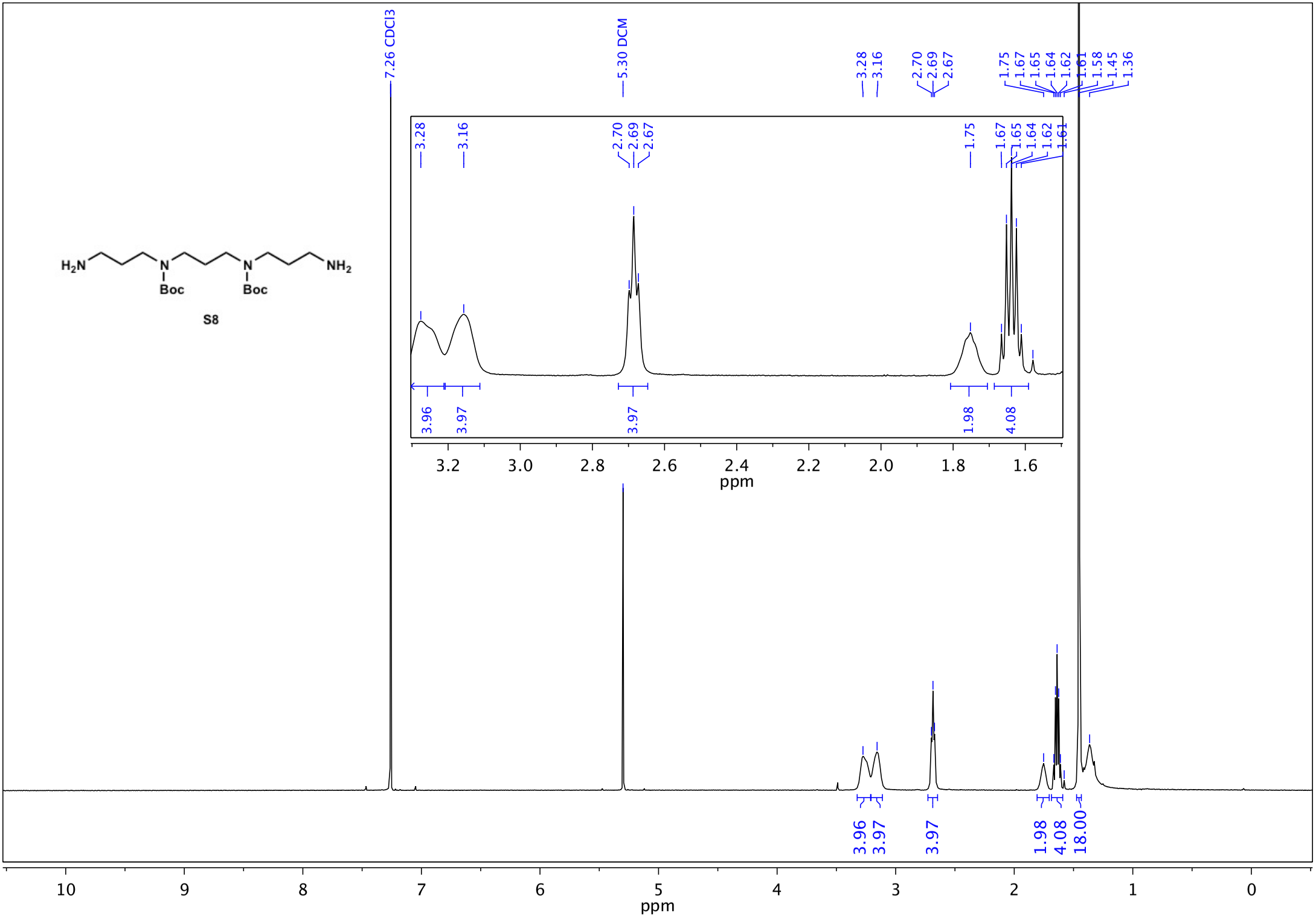
7.26 CDCl3
5.30 DCM
3.28
3.16
2.70
2.69
2.67
1.75
1.67
1.65
1.64
1.62
1.61
1.58
1.45
1.36
3.96
3.97
3.97
1.98
4.08
18.00
ppm
H2N
NH2
N
Boc
Boc
S8

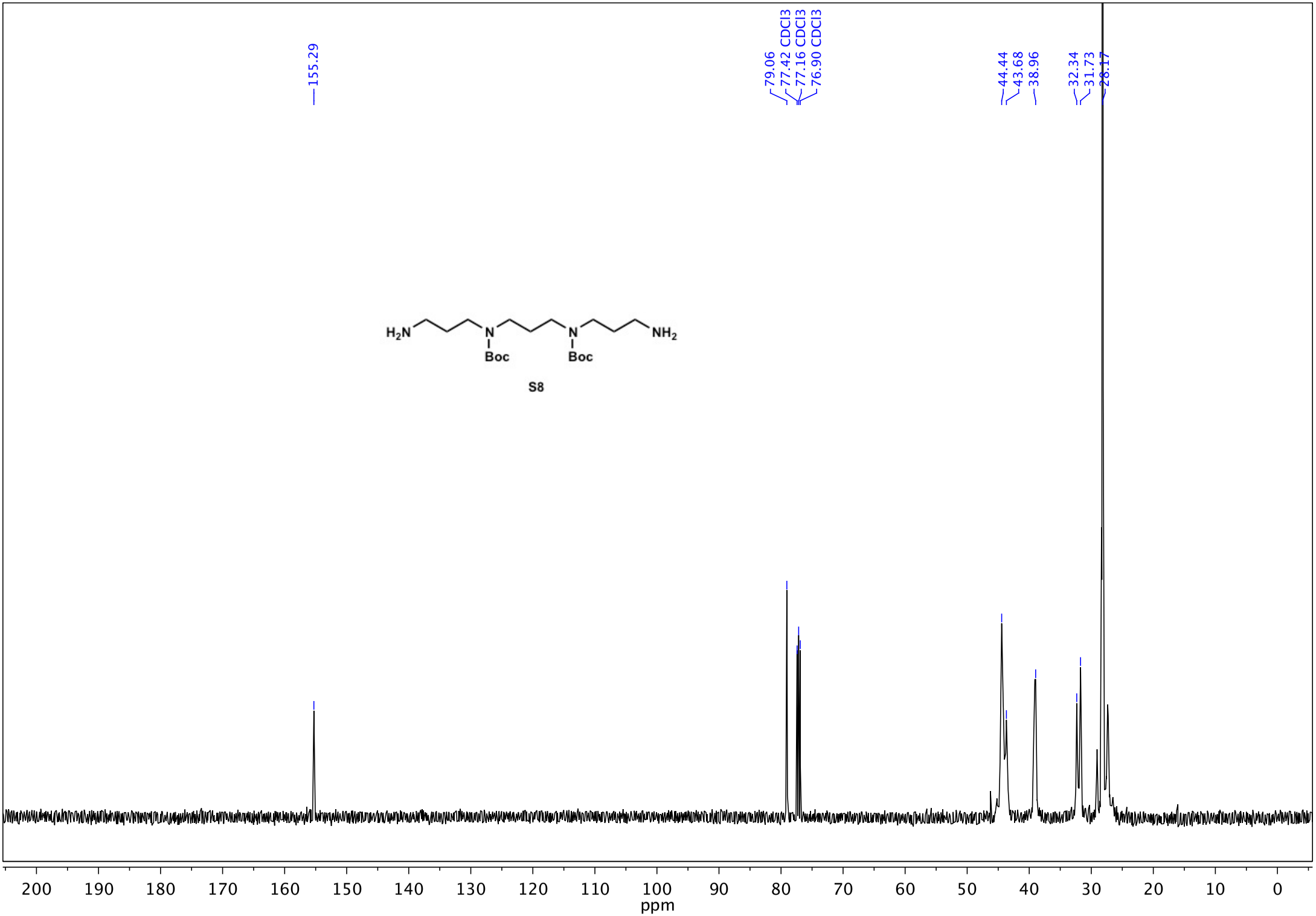
155.29
79.06
77.42 CDCl3
77.16 CDCl3
76.90 CDCl3
44.44
43.68
38.96
32.34
31.73
28.17
H2N
N
Boc
N
Boc
NH2
S8
200
190
180
170
160
150
140
130
120
110
100
90
80
70
60
50
40
30
20
10
0
ppm

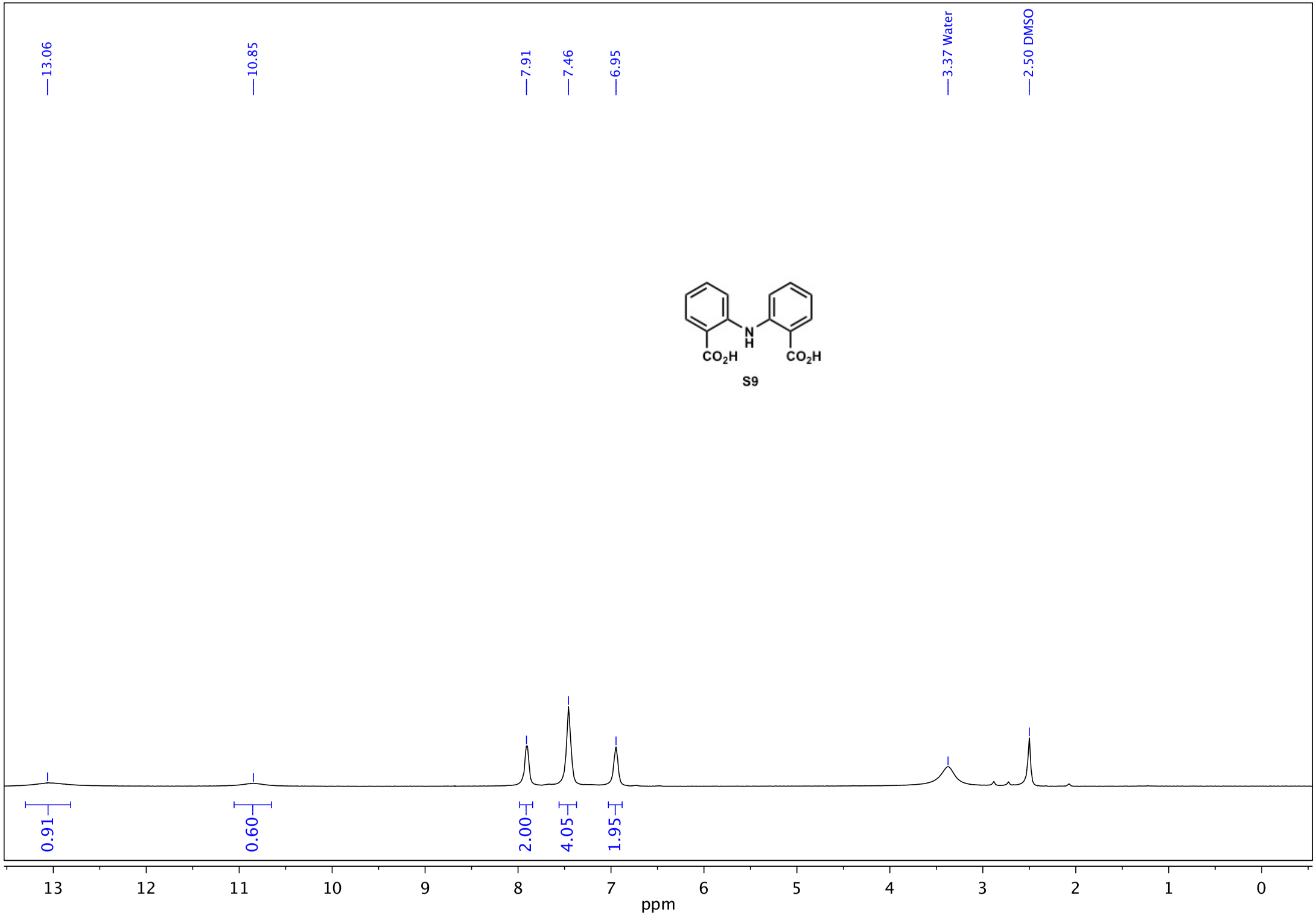
13.06
10.85
7.91
7.46
6.95
3.37 Water
2.50 DMSO
CO2H
N
H
CO2H
S9
0.91
0.60
2.00
4.05
1.95
13
12
11
10
9
8
7
6
5
4
3
2
1
0
ppm

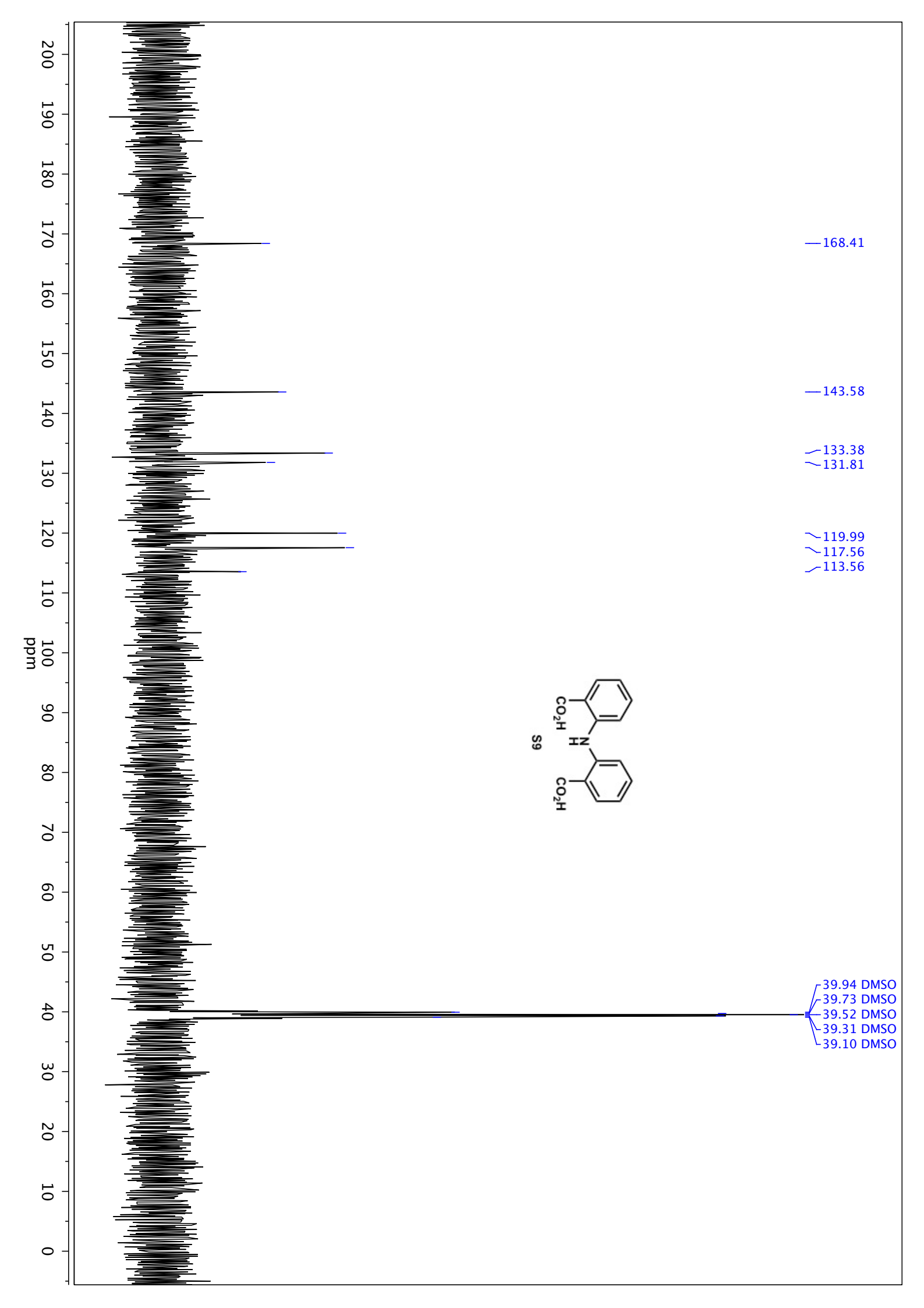
200
190
180
170
160
150
140
130
120
110
100
90
80
70
60
50
40
30
20
10
0
ppm
168.41
143.58
133.38
131.81
119.99
117.56
113.56
39.94 DMSO
39.73 DMSO
39.52 DMSO
39.31 DMSO
39.10 DMSO
CO2H
NH
CO2H
S9

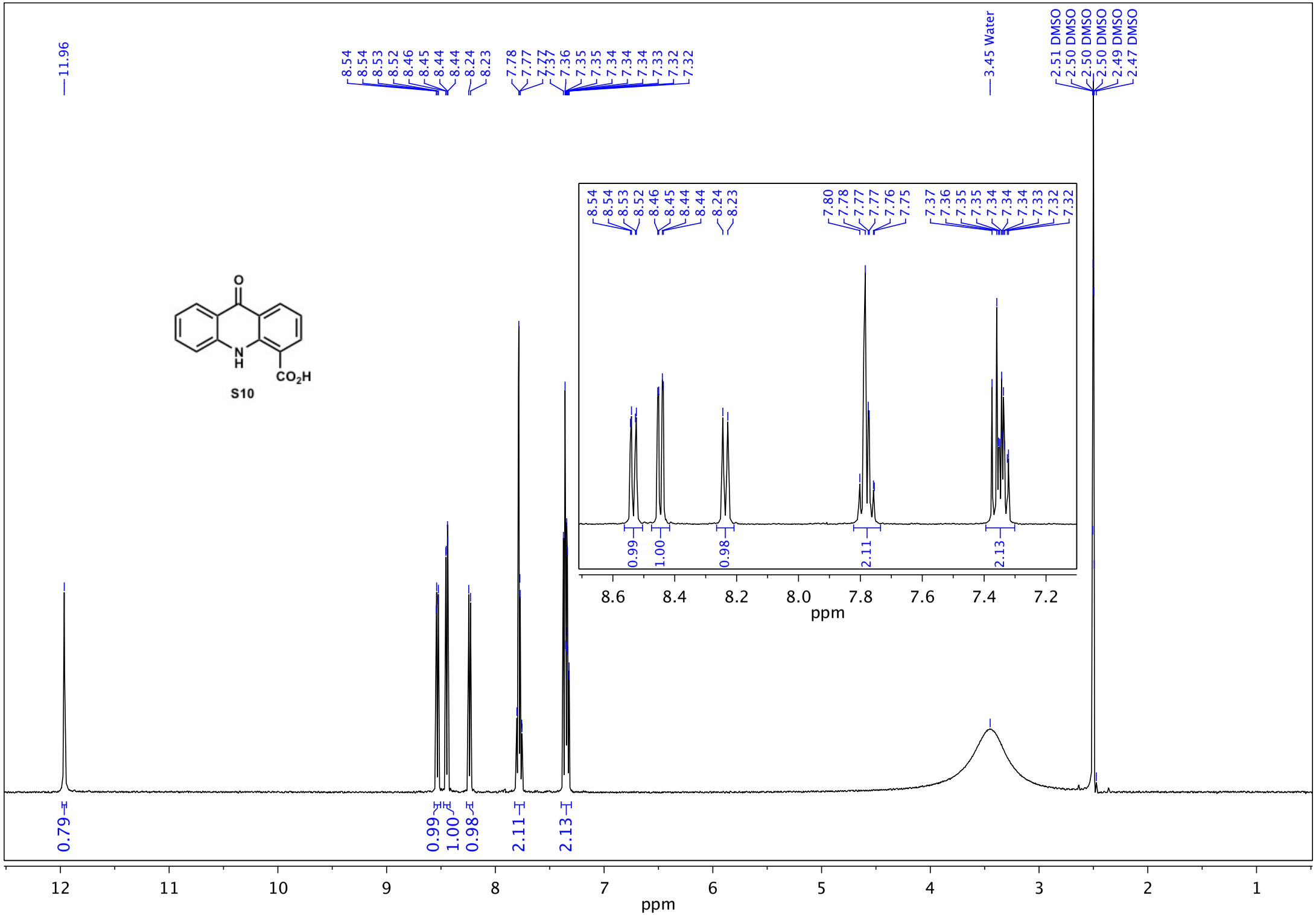
11.96
8.54
8.54
8.53
8.52
8.46
8.45
8.44
8.44
8.24
8.23
7.78
7.77
7.77
7.37
7.36
7.35
7.35
7.34
7.34
7.34
7.33
7.32
7.32
3.45 Water
2.51 DMSO
2.50 DMSO
2.50 DMSO
2.50 DMSO
2.49 DMSO
2.47 DMSO
O
N
H
CO2H
S10
0.79
0.99
1.00
0.98
2.11
2.13
12
11
10
9
8
7
6
5
4
3
2
1
ppm
8.6
8.4
8.2
8.0
7.8
7.6
7.4
7.2
ppm

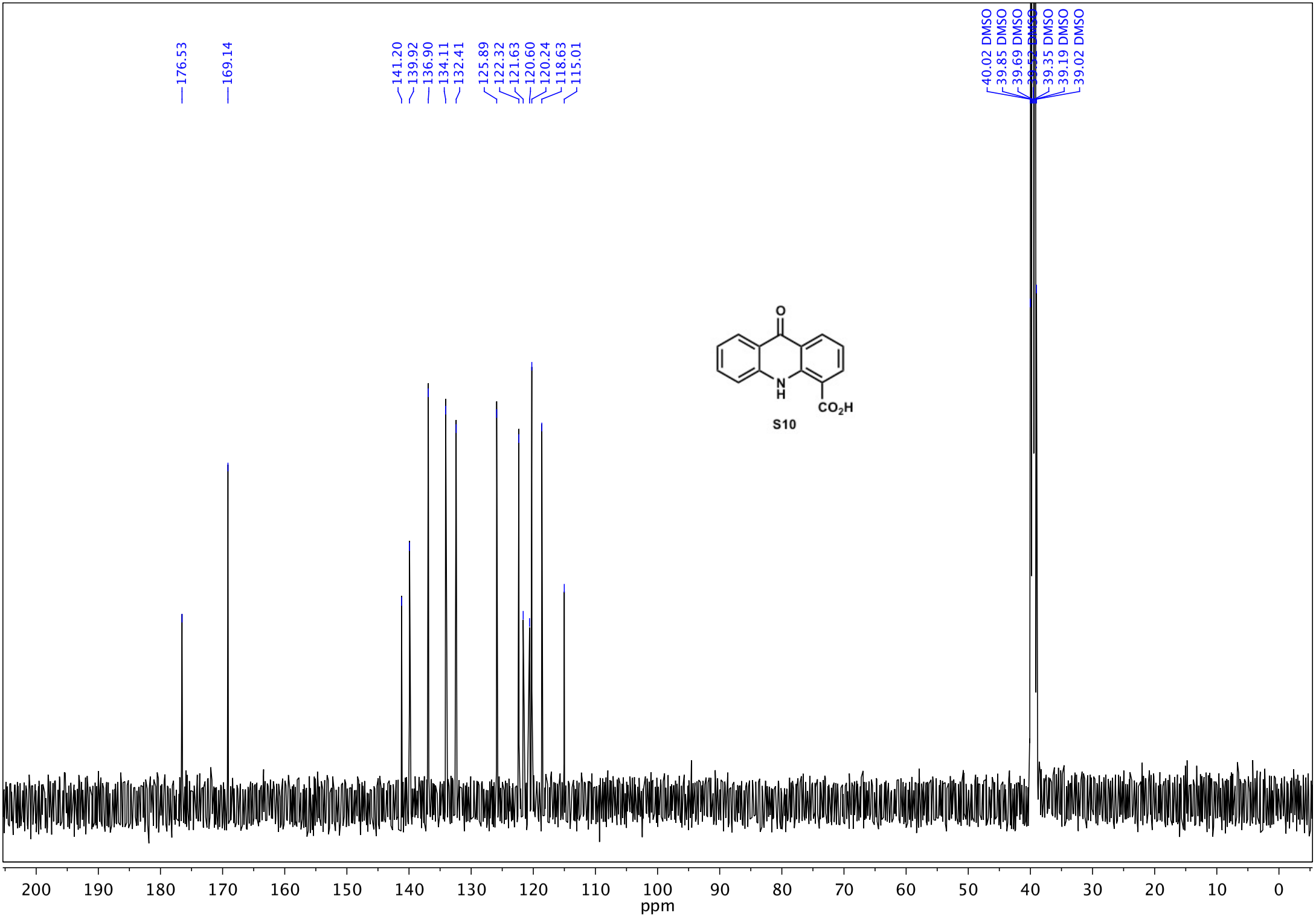
176.53
169.14
141.20
139.92
136.90
134.11
132.41
125.89
122.32
121.63
120.60
120.24
118.63
115.01
40.02 DMSO
39.85 DMSO
39.69 DMSO
39.53 DMSO
39.35 DMSO
39.19 DMSO
39.02 DMSO
O
N
H
CO2H
S10
200
190
180
170
160
150
140
130
120
110
100
90
80
70
60
50
40
30
20
10
0
ppm

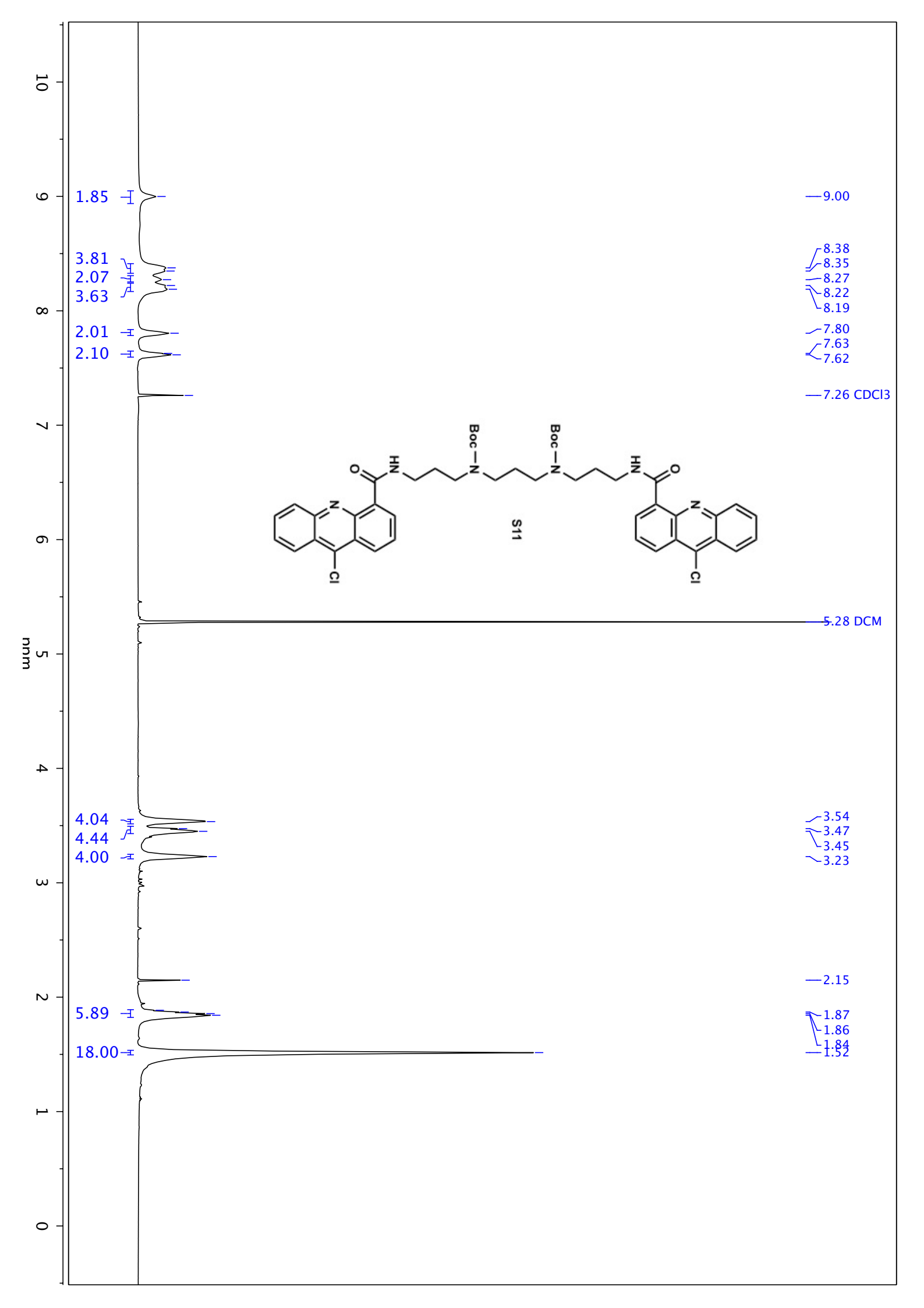
1.85
3.81
2.07
3.63
2.01
2.10
4.04
4.44
4.00
5.89
18.00
9.00
8.38
8.35
8.27
8.22
8.19
7.80
7.63
7.62
7.26 CDCl3
5.28 DCM
3.54
3.47
3.45
3.23
2.15
1.87
1.86
1.84
1.52
Boc—N
Boc—N
HN
HN
O
O
N
N
Cl
Cl
S11
ppm
10
9
8
7
6
5
4
3
2
1
0

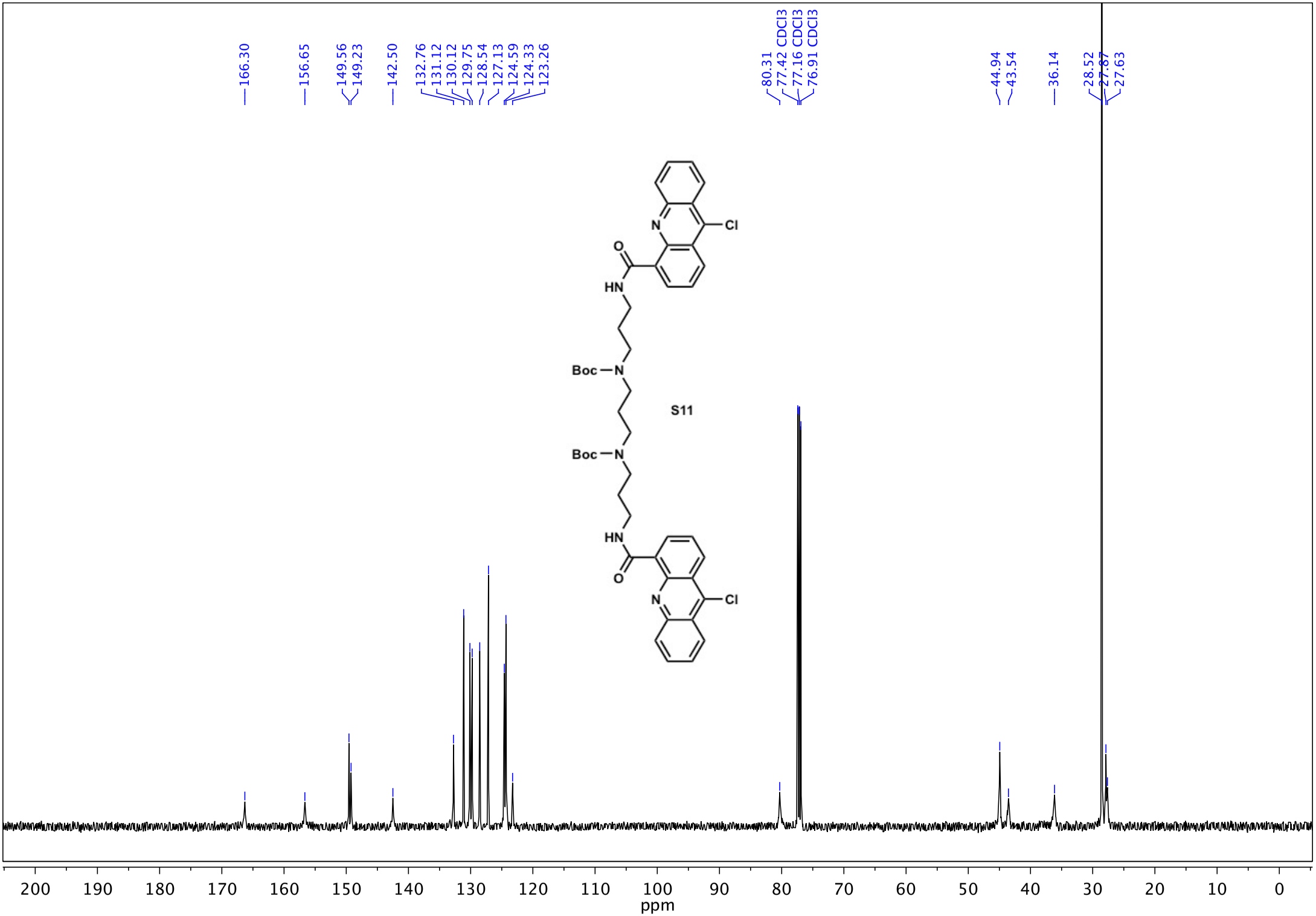
166.30
156.65
149.56
149.23
142.50
132.76
131.12
130.12
129.75
128.54
127.13
124.59
124.33
123.26
80.31
77.42 CDCl3
77.16 CDCl3
76.91 CDCl3
44.94
43.54
36.14
28.52
27.87
27.63
Cl
O
HN
Boc
N
S11
200
190
180
170
160
150
140
130
120
110
100
90
80
70
60
50
40
30
20
10
0
ppm

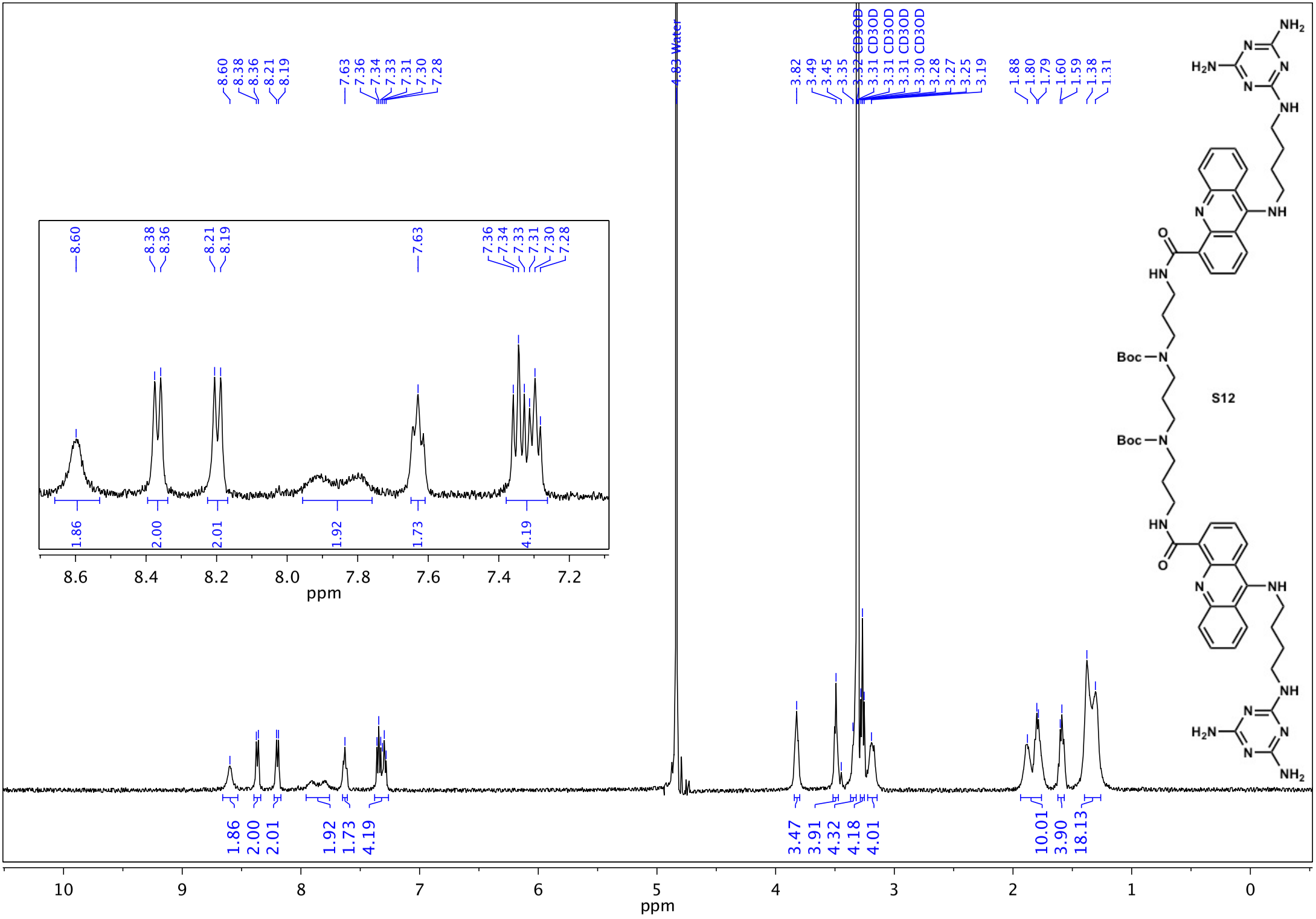
8.60
8.38
8.36
8.21
8.19
7.63
7.36
7.34
7.33
7.31
7.30
7.28
4.83 Water
3.82
3.49
3.45
3.35
3.32 CD3OD
3.31 CD3OD
3.31 CD3OD
3.31 CD3OD
3.30 CD3OD
3.28
3.27
3.25
3.19
1.88
1.80
1.79
1.60
1.59
1.38
1.31
1.86
2.00
2.01
1.92
1.73
4.19
3.47
3.91
4.32
4.18
4.01
10.01
3.90
18.13
ppm
S12

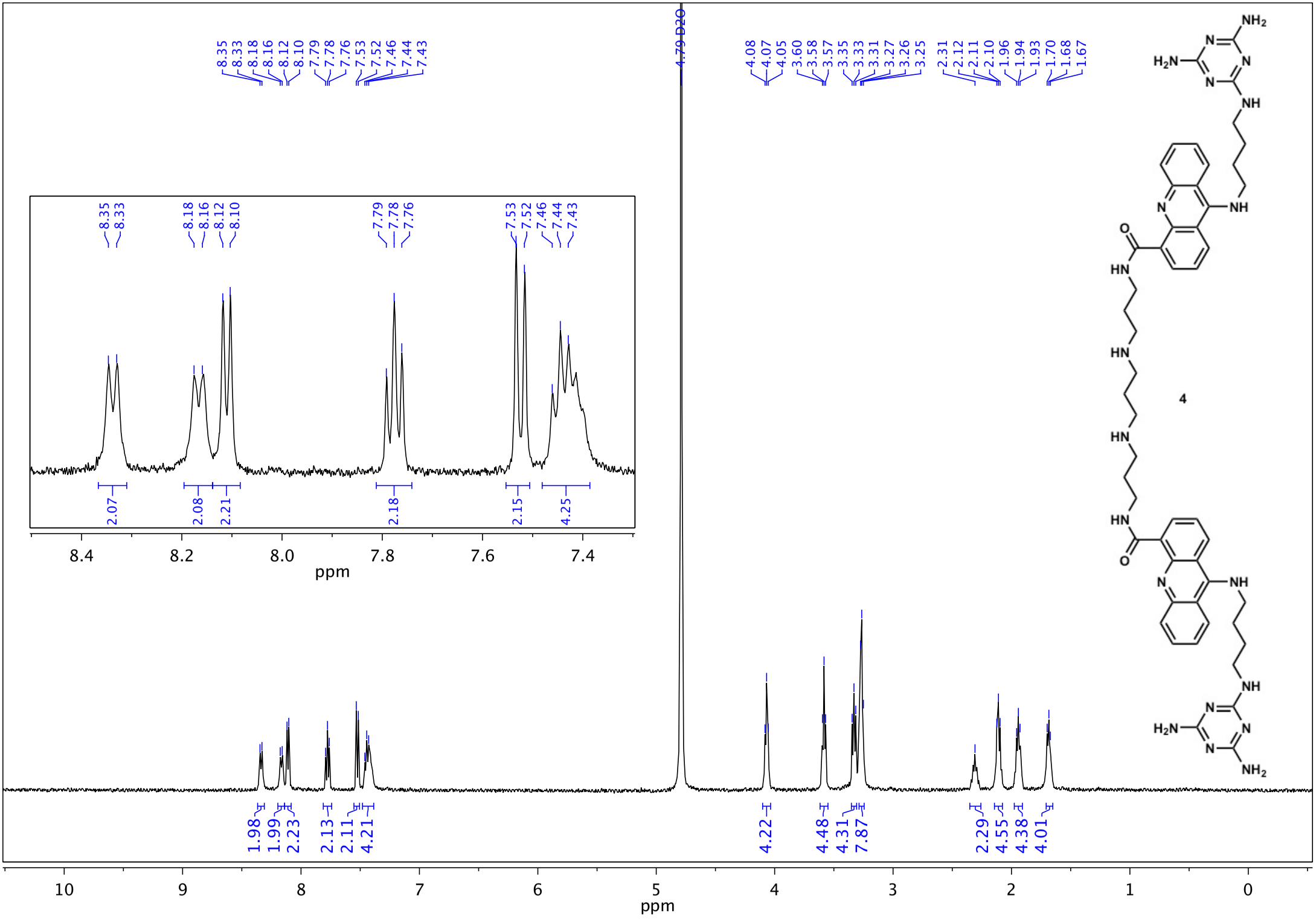
8.35
8.33
8.18
8.16
8.12
8.10
7.79
7.78
7.76
7.53
7.52
7.46
7.44
7.43
4.79 D2O
4.08
4.07
4.05
3.60
3.58
3.57
3.35
3.33
3.31
3.27
3.26
3.25
2.31
2.12
2.11
2.10
1.96
1.94
1.93
1.70
1.68
1.67
2.07
2.08
2.21
2.18
2.15
4.25
8.4
8.2
8.0
7.8
7.6
7.4
ppm
1.98
1.99
2.23
2.13
2.11
4.21
4.22
4.48
4.31
7.87
2.29
4.55
4.38
4.01
10
9
8
7
6
5
4
3
2
1
0
ppm
4